CALIFORNIA ENERGY COMMISSION

ENERGY RESEARCH AND DEVELOPMENT DIVISION

FINAL PROJECT REPORT

Development of an Integrated Methodology for Assessing Integrity of Levees Protecting Fossil Gas Infrastructure

August 2024 | CEC-500-2024-093

PREPARED BY:

Ozgur Kozaci InfraTerra, Inc.
Primary Author

Scott Brandenberg, University of California, Los Angeles

Roland Burgmann, University of California, Berkeley

Mitchell Craig, California State University, East Bay

Koichi Hayashi, Geometrics

Christopher Hitchcock, InfraTerra, Inc.

Xie Hu, University of California, Berkeley

Joe O’Hagan
Project Manager
California Energy Commission

Agreement Number: PIR-17-013

Alexandra Horangic
Branch Manager
SUSTAINABILITY AND RESILIENCE BRANCH

Jonah Steinbuck, Ph.D.
Director
ENERGY RESEARCH AND DEVELOPMENT DIVISION

Drew Bohan
Executive Director

ACKNOWLEDGEMENTS

Cathleen Jones of NASA JPL and Jeffrey Bachhuber of PG&E Geosciences provided expert review as part of the Technical Advisory Committee.

PREFACE

The California Energy Commission's (CEC) Energy Research and Development Division manages the Gas Research and Development Program, which supports energy-related research, development, and demonstration not adequately provided by competitive and regulated markets. These natural gas research investments spur innovation in energy efficiency, renewable energy and advanced clean generation, energy-related environmental protection, energy transmission and distribution and transportation.

The Energy Research and Development Division conducts this public interest natural gas-related energy research by partnering with RD&D entities, including individuals, businesses, utilities and public and private research institutions. This program promotes greater gas reliability, lower costs and increases safety for Californians and is focused in these areas:

- Buildings End-Use Energy Efficiency
- Industrial, Agriculture and Water Efficiency
- Renewable Energy and Advanced Generation
- Natural Gas Infrastructure Safety and Integrity
- Energy-Related Environmental Research
- Natural Gas-Related Transportation

Development of an Integrated Methodology for Assessing Integrity of Levees Protecting Fossil Gas Infrastructure is the final report for PIR-17-013, conducted by InfraTerra, Inc. The information from this project contributes to the Energy Research and Development Division's Gas Research and Development Program.

For more information about the Energy Research and Development Division, please visit the CEC's research website (www.energy.ca.gov/research/) or contact the Energy Research and Development Division at ERDD@energy.ca.gov.

ABSTRACT

At the confluence of the Sacramento and San Joaquin rivers lies a complex system of over 1,100 miles of levees — longer than California's coastline. Many levees are a century old, surrounding hundreds of thousands of acres of land, and mostly below sea level. This area is a major hub of fossil gas and electricity infrastructure, containing significant fossil gas production and underground storage fields, and it is crossed by major electricity transmission lines and fossil gas pipelines.

Levees in the Sacramento-San Joaquin Delta were built as simple peat dikes resting on marsh soils and are therefore highly vulnerable to damage from floods, wave action, seepage, subsidence, burrowing animals, earthquakes, and sea level rise. The structural integrity of levees in the Sacramento-San Joaquin Delta (Delta) has for decades been a subject of investigations and continues to be a source of concern. This project identified areas of high risk to fossil gas infrastructure in the Delta and tested multiple geophysical methods for assessing levee integrity at several Delta sites. Methods include remote sensing and seismic surface wave surveying, electrical resistivity, ground penetrating radar, and electromagnetic surveying. Geotechnical models developed for assessing levee failure modes and characterizing variability along levees incorporate the geophysical and remote sensing data.

Keywords: levee failure, Sacramento-San Joaquin Delta, fossil gas infrastructure, remote sensing and seismic surface wave surveying, electric resistivity, ground penetrating radar, electromagnetic surveying

Please use the following citation for this report:

Kozaci, Ozgur. 2024. *Development of an Integrated Methodology for Assessing Integrity of Levees Protecting Fossil Gas Infrastructure*. California Energy Commission. Publication Number: CEC-500-2024-093.

TABLE OF CONTENTS

LIST OF FIGURES

LIST OF TABLES

Executive Summary

This research consists of the development of non-invasive geophysical data acquisition technologies for conditions specific to levees in the Sacramento-San Joaquin Delta (Delta) and for evaluating threats to fossil gas infrastructure. The methodology for this research aims to improve characterization of spatial variability of soil deposits associated with levee systems, to improve risk assessment for major threats from increased flooding and sea level rise associated with climate change in northern California.

Background

As part of California's broader efforts to combat climate change and achieve carbon neutrality by 2045, the state seeks to reduce its dependence on fossil gas. A significant portion of the state, however, still depends on fossil gas. It is critical that the fossil gas infrastructure continues to function safely and efficiency while the state is in transition to a zero-carbon energy system.

The structural integrity of levees in the Delta is critical to protecting people, property, man-made infrastructure, natural resources, and California's water supply. A network of 1,115 miles of levees protects about 700,000 acres of lowland in the Delta. This network is the first line of defense against flooding for a major hub of fossil gas infrastructure in the Delta, including transmission pipelines and storage.

Delta levees are vulnerable to damage from floods, wave action, seepage, subsidence, earthquakes, and sea level rise. The importance and benefits of informed fossil gas system integrity management in the Delta are three-fold: (1) the safety and reliability of the fossil gas supply are essential for economic and residential sustainability; (2) the economic impact of failures to the fossil gas system and the transportation network in which it is embedded can be significant to the industry and residents; (3) product releases in the Delta can impact air quality and regulatory goals related to carbon emissions. Proactive mitigation of hazards through a phased and targeted approach prevents disturbances to business and residential customers through reliability and avoids costly emergency response expenditures in response to unforeseen failures.

Project Purpose and Approach

The research methodology improves characterization of the spatial variability of soil deposits associated with levee systems in the Delta, which is necessary to assess the risk of levee failure. The project included testing an array of geophysical methods (seismic surface wave, electrical resistivity, ground penetrating radar, and electromagnetic) at select sites representing similar conditions. This approach yields two types of benefits: (1) geophysical methods are tested in a range of environments specific to the Delta and acquisition parameters are fine-tuned specifically for this environment; and (2) it enables refinement of input into the geohazard layers with high-resolution site-specific data.

Use of an integrated geophysical acquisition approach utilizing complementary techniques provides more reliable results than would any single data acquisition technology. Uncertainties inherent in geophysical imaging stem from the compromise between resolution versus penetration at varying degrees in heterogeneous physical conditions. Optimizing the complementary geophysical techniques, in combination with acquisition design, enhances resolution and penetration while reducing uncertainties.

Multi-method near-surface geophysical surveys were performed to evaluate the structural integrity of levees at McDonald Island within the Delta. Priority was given to sites where levee failure would compromise gas pipelines or other gas infrastructure. Sites were selected after review of soil borehole logs, topographic maps, flood inundation maps, liquefaction susceptibility maps, soil maps, aerial imagery, and interferometric synthetic aperture radar data. Pacific Gas & Electric was a key project partner in this study.

Key Results

The project identified areas of high risk to fossil gas infrastructure in the Delta and tested multiple geophysical methods to assess levee integrity.

Combined interpretation of optical and microwave remote sensing images from the ground, air, and space, calibrated by a dense monitoring network of in-situ geophysical and geotechnical tools, can help improve understanding of the spatiotemporal development of the levee systems. Resolving localized deformation in the delta environment is challenging, due to constantly changing soil moistures and vegetated covers from agricultural harvest and seasonal growth, as well as atmospheric turbulence. A suggested temporal threshold for C-band spaceborne Sentinel-1 data is less than one month, to maintain the coherence in the Delta. A regional displacement pattern over the Delta was quantified, highlighting an increasing subsidence to the south, where groundwater depletion occurs in the San Joaquin Valley.

As a complement, interferometric synthetic aperture radar coherence and synthetic aperture radar amplitude were increasingly used to unveil land cover changes and soil-moisture-related processes. The change of amplitude dispersion showed two linear features southwest of McDonald Island that we interpreted to be due to road widening. Repeated harvests could be effectively located and traced as well.

Another key finding is that the horizontal variability of the levee as indicated by seismic S-wave velocity was much more rapid in the levee body (upper 3 meters) than in the geologic substrate.

Knowledge Transfer and Next Steps

Results from seismic surveys for this project were published in an article in the journal *Near Surface Geophysics*.

To build on the results of this project, additional detailed risk analyses of the levees can be conducted by running the updated geotechnical models developed by this project in the Open System for Earthquake Engineering Simulation. Open System for Earthquake Engineering

Simulation is a software framework for developing applications to simulate the performance of structural and geotechnical systems subjected to earthquakes.

CHAPTER 1: Introduction

The approximately 3,000-square-kilometer (km^2) Sacramento-San Joaquin Delta (Delta), made up of approximately 70 major islands (Sharma et al., 2016), is the largest estuary along the west coast of the United States (U.S. Geological Survey, 2013). Most of the islands' elevations are below sea level. Persistent ground subsidence has been observed since the late 1800s, when reclamation started, in the forms of controlled burning and water drainage for agriculture and levee/embankment construction (Sharma et al., 2016). The accompanying release of carbon dioxide (CO_2) and soil degradations further contributed to the sinking Delta (Ingebritsen et al., 2000; U.S. Geological Survey, 2013). A local sea-level rise at a rate of approximately 2 millimeters per year (mm/yr) could further hasten the arrival of seawater intrusion.

Remote sensing results have highlighted the subsidence of Sherman Island in the westernmost section of the Delta, which stands between the saline ocean water from the San Francisco Bay and the rest of the Delta (Deverel et al., 2016; NASA, 2017). Sherman Island subsided at 13 mm/yr plus or minus (±) 2 mm/yr during 2009-2014 (Sharma et al., 2016); and, just west of the island, the peak subsidence rate reached as high as 160 mm/yr ± 4.4 mm/yr during 2009-2015 (Bekaert et al., 2019). On average, the Delta is subsiding at a rate of 9.2 mm/yr ± 4.4 mm/yr (Bekaert et al., 2019).

In the context of the active Hayward-Calaveras fault zone and other East Bay faults, the Delta is threatened by seismic-induced failure (Jones et al., 2016). All these factors make the estuary especially vulnerable to inundation and land loss. Monitoring the stability of the earthen levees in the estuary has become a significant societal need (An et al., 2020). Because the network of Delta levees provides a first line of defense against flooding for a major hub of gas infrastructure in the Delta, including transmission pipelines and storage, monitoring levee stability is important for providing fossil gas ratepayers with safe, reliable service.

CHAPTER 2: Project Approach

This project benefited from the engagement of its Technical Advisory Committee, which included the active participation, including technical review of findings, of Pacific Gas & Electric and the National Aeronautics and Space Administration Jet Propulsion Laboratory (NASA JPL).

GIS Data Compilation

As part of the project, existing geologic, geophysical, soil, and elevation datasets were integrated into a comprehensive geographical information system (GIS) database that includes three major data sets: geohazards, levee condition, and fossil gas infrastructure. These data sets were combined to develop a map that delineates the Delta area into distinct regions with similar cumulative susceptibility for detailed geophysical data acquisition.

Remote Sensing

Geotechnical instruments (such as borehole, tiltmeter, and creepmeter), geophysical surveys (such as seismic, electrical resistivity tomography, fiber-optics), and geodetic tools (such as global navigation satellite system; Global Positioning System; and laser imaging, detection, and ranging [LiDAR]) were used to retrieve the physical properties and to infer the structural integrity of the levee systems. However, these field-based approaches are labor intensive and costly.

As an active remote sensing tool operating at microwave wavelength, synthetic aperture radar (SAR) transmits electromagnetic waves to the ground and receives the echoes backscattered from the ground. The complex format radar signals can be interpreted as amplitude and phase. Amplitude mainly characterizes the physical properties of the ground objects, and phase is determined by the traveling distance of the electromagnetic waves.

The application of interferometric synthetic aperture radar (InSAR) in the Delta is challenged by phase decorrelation due to tidal marshes, wetlands, and reclaimed lands, especially when using relatively shorter-wavelength C-band data (Cohen et al., 1998; Brooks et al., 2012). For this non-urban landscape, L-band uninhabited aerial vehicle synthetic aperture radar (UAVSAR) data have the advantage of longer-wavelength acquisitions, but the revisit time is on the timescale of months. The airborne and spaceborne SAR data, the Shuttle Radar Topography Mission (SRTM) digital elevation dataset, and the LiDAR digital elevation model (DEM) were jointly used to evaluate the stability of the Delta and its levee system.

UAVSAR is operated by JPL/NASA. This L-band system (wavelength: 0.238 meters [m]) was repeatedly deployed over the Delta every one-half month to two months. As an airborne imaging system, UAVSAR has small single-look pixel spacings of 0.6m and 1.67m in azimuth and range directions, respectively. For this non-urban landscape, L-band UAVSAR data have the advantage of longer-wavelength acquisitions.

Geophysical Surveys

Near surface geophysical surveys were conducted to evaluate the structural integrity of levees at McDonald Island (Figure 1), where levee failure would compromise gas pipelines and other gas infrastructure. Methods included seismic surface wave, electrical resistivity, ground penetrating radar (GPR), and magnetic. Geophysical survey sites were selected after review of soil borehole logs, topographic maps, soil maps, aerial imagery, and InSAR data. The position of geophysical surveys was tied to Department of Water Resources (DWR) distance posts on the levee road with measuring tape. Point locations were also recorded using GPS and used to assign global coordinates.

Figure 1: Satellite Image of McDonald Island Showing the Sites of Geophysical Surveys

The seismic surface wave method was used to obtain estimates of shear wave velocity (Vs). Electrical resistivity surveys were used to distinguish between sandy and clayey soils. GPR provided detailed images of stratigraphy that may help locate parts of the levee affected by rodent burrows. Magnetic surveys were used to verify the location of fossil gas supply pipelines and irrigation drains (sumps).

Seismic surveys were carried out at selected locations on McDonald Island, along both the top and the bottom of the perimeter levee using the surface wave method. More specifically, the two-dimensional multichannel analysis of surface waves (2D MASW) method was used. Seismic surveys were performed using a land streamer to obtain Vs estimates within the levee body and beneath the levee. Of the different geophysical methods used in this study, the seismic method was the most time and labor intensive; however, it provided an essential indicator of levee integrity, the Vs.

Passive surveys were performed along the base of the levee using cableless seismographs (Geometrics Atom), each with a 2-hertz (Hz) geophone, to record ambient noise. A total of 30 seismograph units were used, with a receiver spacing of 5 m, providing a spread length of 145 m. The sample interval was 4 m. The record length was 30 minutes to 60 minutes for each patch. The spread was rolled 2 to 3 times, each time with 50 percent overlap.

Seismic waveform data was used to determine a one-dimensional (1D) velocity depth profile at each location along the levee, and the 1D profiles were combined to produce a 2D profile. Active and passive data were processed separately through the preparation of frequency-velocity spectra and the picking of dispersion curves. Active data were processed using the common midpoint cross correlation (CMP-CC) method. Passive data were processed using the common midpoint spatial autocorrelation (CMP-SPAC) method.

Both active and passive data were first sorted into common midpoint (CMP) gathers using a 10-m bin size. Active and passive data from each location were processed to produce a combined dispersion curve and 1D velocity-depth profile.

Electrical resistivity surveys were carried out using a capacitively-coupled dipole (CCD) system to complement seismic surveys. The CCD system is towed while data is recorded, which allows for a very high rate of data acquisition. Magnetic and GPR surveys were carried out using wheeled carts, and they also have high rates of data acquisition.

Levee Stability Risk Assessment

Risk assessment for levee systems generally involves assigning fragility functions characterizing the capacity of levee segments, assessing the demand imposed on each segment by an initiating event, computing the probability of failure of segments within a reach, and subsequently assessing the consequences of failure.

Soil properties within levees are spatially variable due to construction sequence, availability of fill material, and other factors. Spatial variability cannot be accurately quantified using traditional geotechnical site investigation methods, but it can potentially be quantified using geophysical methods. Spatial variability is an important aspect of levee stability.

A set of slope stability simulations illustrates the influence of spatial variability on levee stability. Both homogeneous and spatially variable models were being developed to demonstrate the influence of material heterogeneity on failure. Once critical model elements were identified, these findings would provide guidance for geophysical methods in targeting specific parameters. The research team validated the proposed method of random field generation and applied it to a levee model that might be of more interest.

The research team started with a simple levee model and finite element mesh, as shown in Figure 2. This mesh was created using GiD[1], which is a pre- and post-processor for numerical simulations. The research team was also able to export the mesh information from GiD (Figure 2), which could be used to generate a random field of undrained strength by using the

[1] GiD is a universal, adaptive and user-friendly pre and post processor for numerical simulations in science and engineering. It has been designed to cover all the common needs in the numerical simulations field from pre to post-processing. https://www.gidsimulation.com/

proposed method. Undrained strength is the maximum shear stress that soil can withstand without experiencing any change in its volume in undrained conditions. Different random field properties could be assigned to different parts of the levee with the use of the random field generation method. Figure 3 is an example of a contour map of the undrained strength, showing spatially correlated random fields within the levee and in the foundation. Spatial correlation was applied separately within these regions, whereas the properties within the levee were uncorrelated with the properties in the foundation. The goal (for future research) is to develop procedures to run a dynamic analysis for such a levee with assigned soil properties in OpenSees[2].

Figure 2: A Sketch of a Levee Model with Generated Mesh by GiD

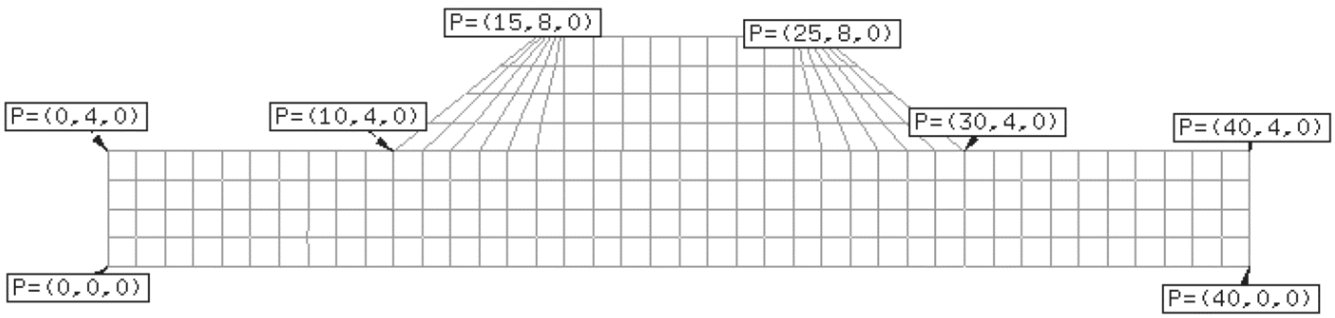

Figure 3: High-density Point Cloud Data for McDonald Island Site 1

[2] A software framework for developing applications to simulate the performance of structural and geotechnical systems subjected to earthquakes. A number of OpenSees applications are released on this website: https://opensees.berkeley.edu/

CHAPTER 3: Results

For this study, integration and analysis of existing geologic, geophysical, soil, and elevation datasets were used to characterize delta conditions and to guide geophysical testing site selection. Historic topographic maps from the United States Geological Survey (USGS) 7.5′ quadrangle series were reviewed for information on modifications to the island and the rate of subsidence. Four quadrangles intersect on McDonald Island at 38°00′ north and 121°30′ west. The 1910 Headreach (now Terminous) quadrangle shows the northern portion of McDonald Island as undeveloped tidal marsh, with no evidence of alterations to meandering tidal channels, including the northern end of Whiskey Slough. See Figure 4, which shows (left) unified soil classification units on and in the vicinity of McDonald Island and (right) distribution of percent peat across and in the vicinity of McDonald Island.

Figure 4: Samples of GIS Database Layers from U.S. Dep. of Agriculture (USDA) Soil Survey Geographic Database

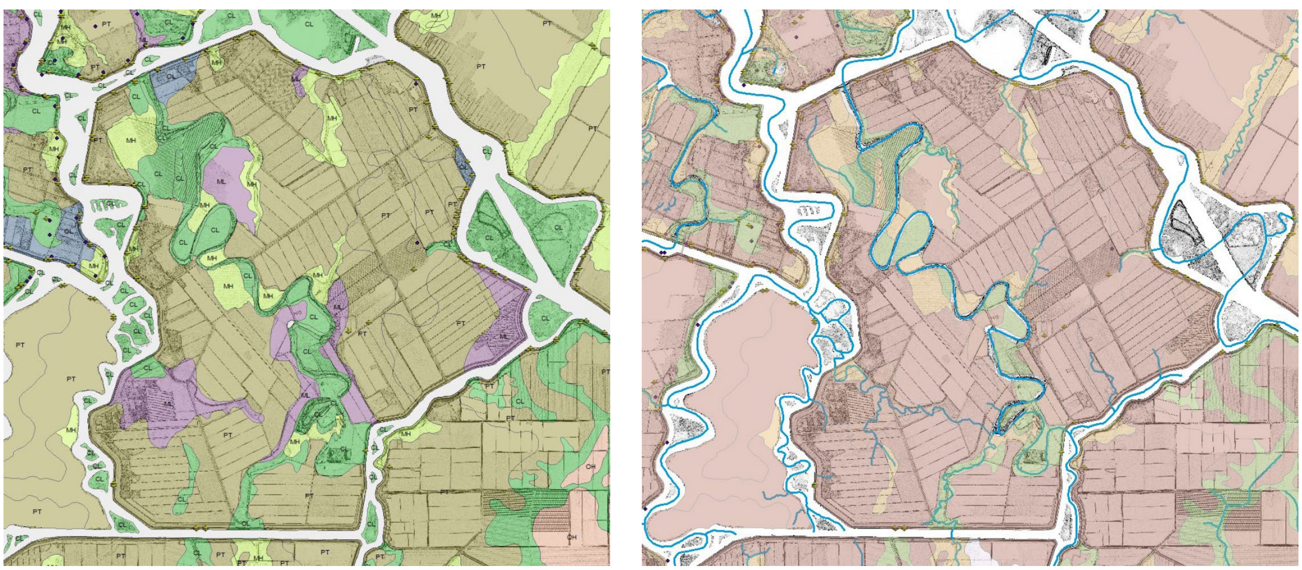

The research team selected and prioritized more than ten sites for the planned geophysical data acquisition on McDonald Island. The site selection and prioritization considered various geologic levee conditions (e.g., buried channel crossing under levees), existing infrastructure locations (levee — pipe crossings), availability of subsurface information (e.g., borehole logs), and preliminary results of InSAR analysis. The research team acquired high-resolution aerial photographs of the survey locations via a drone platform and processed the data to develop high-density point clouds, DEMs, and high-resolution orthophoto mosaics.

To finish building up a levee cross-section in McDonald Island, a location was selected as close as possible to the boring log locations, so the information from the borings could be incorporated into the finite element model. Figure 5 shows the digital elevation model and orthomosaic for the McDonald Island site 1. Figure 6 shows the approximate location of the cross-section selected, and the lower part of the figure shows the geometry profile at that cross-section. The horizontal axis is in meters and the vertical axis is in feet. The research team was able to subsample points shown in Figure 7 to be imported into GiD to generate mesh. Figure 8 shows two boring logs from the levee cross-section that provided the boring log information that were incorporated into the soil stratigraphy profile.

Figure 5: Digital Elevation Model (DEM) (left) and Orthomosaic (right) for McDonald Island Site 1

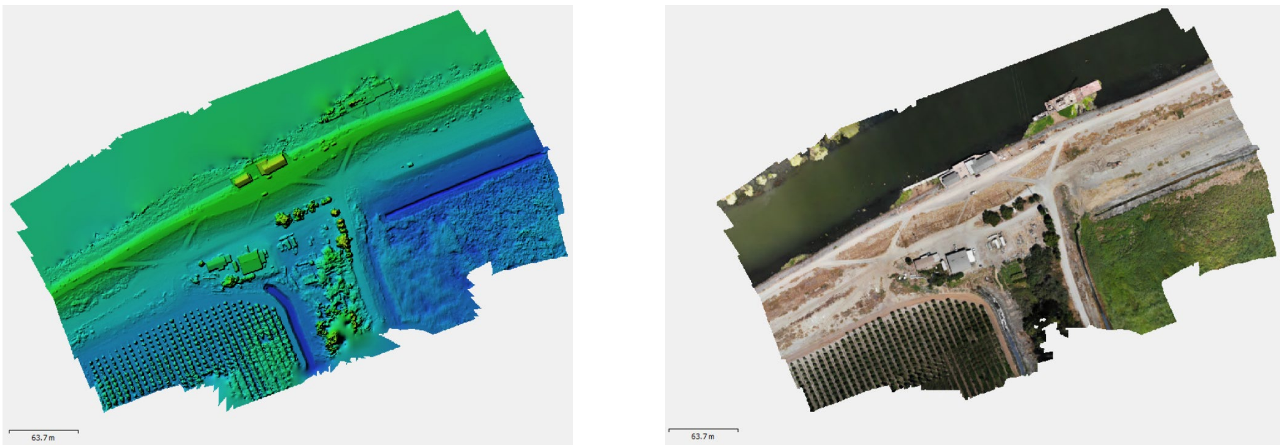

Figure 6: One Cross-section Profile

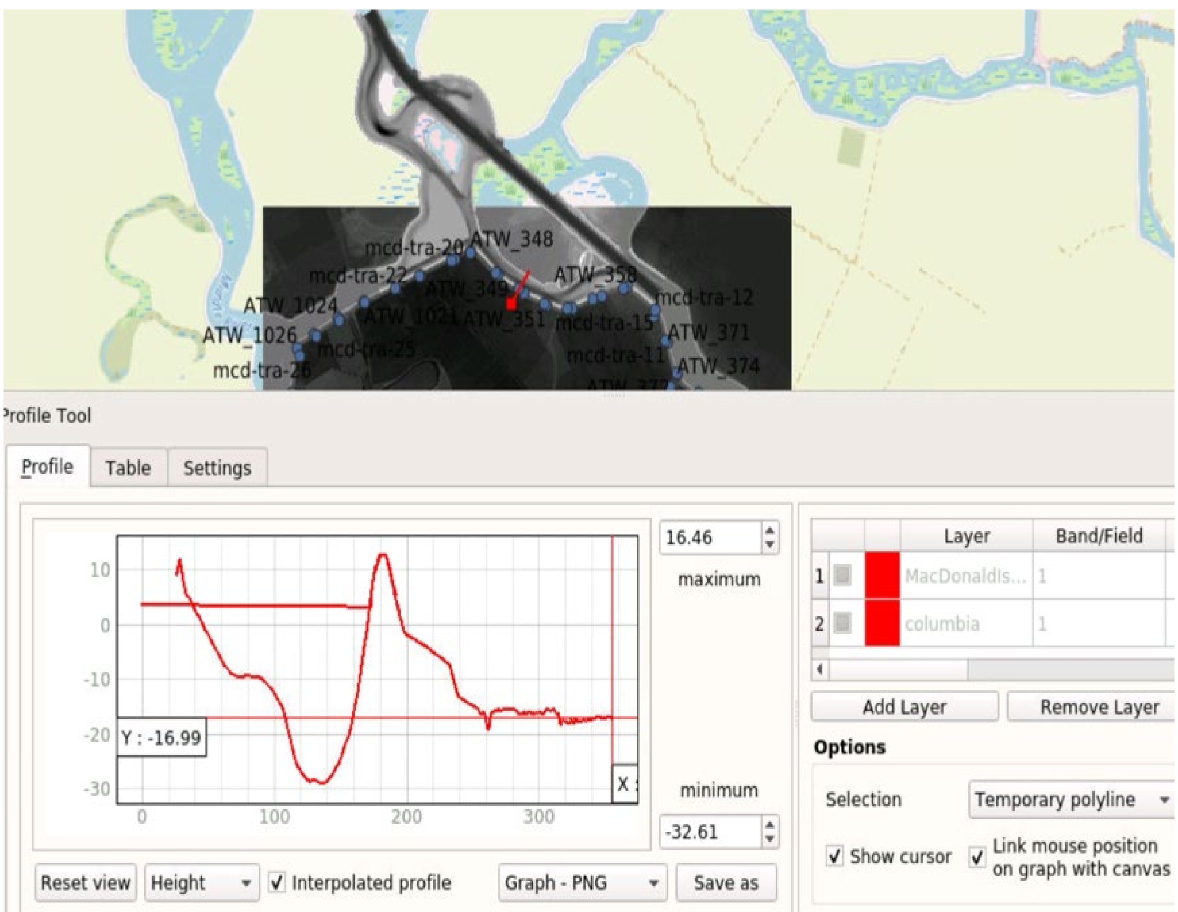

Figure 7: Points Used for the Cross-section Geometry

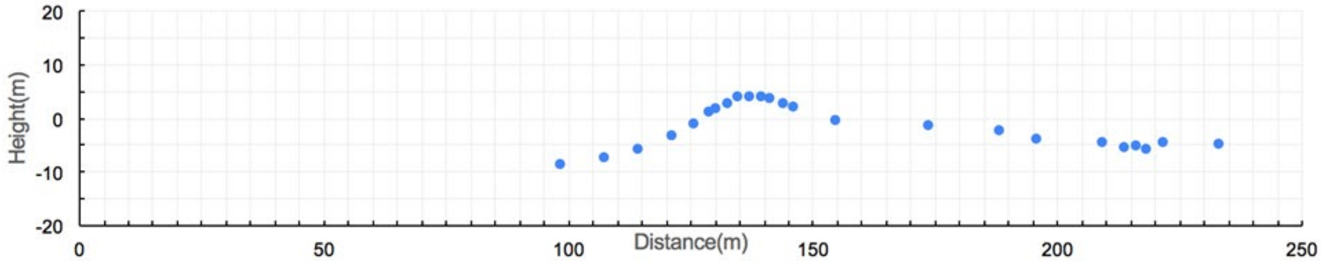

Figure 8: Two Boring Logs at the Cross-section

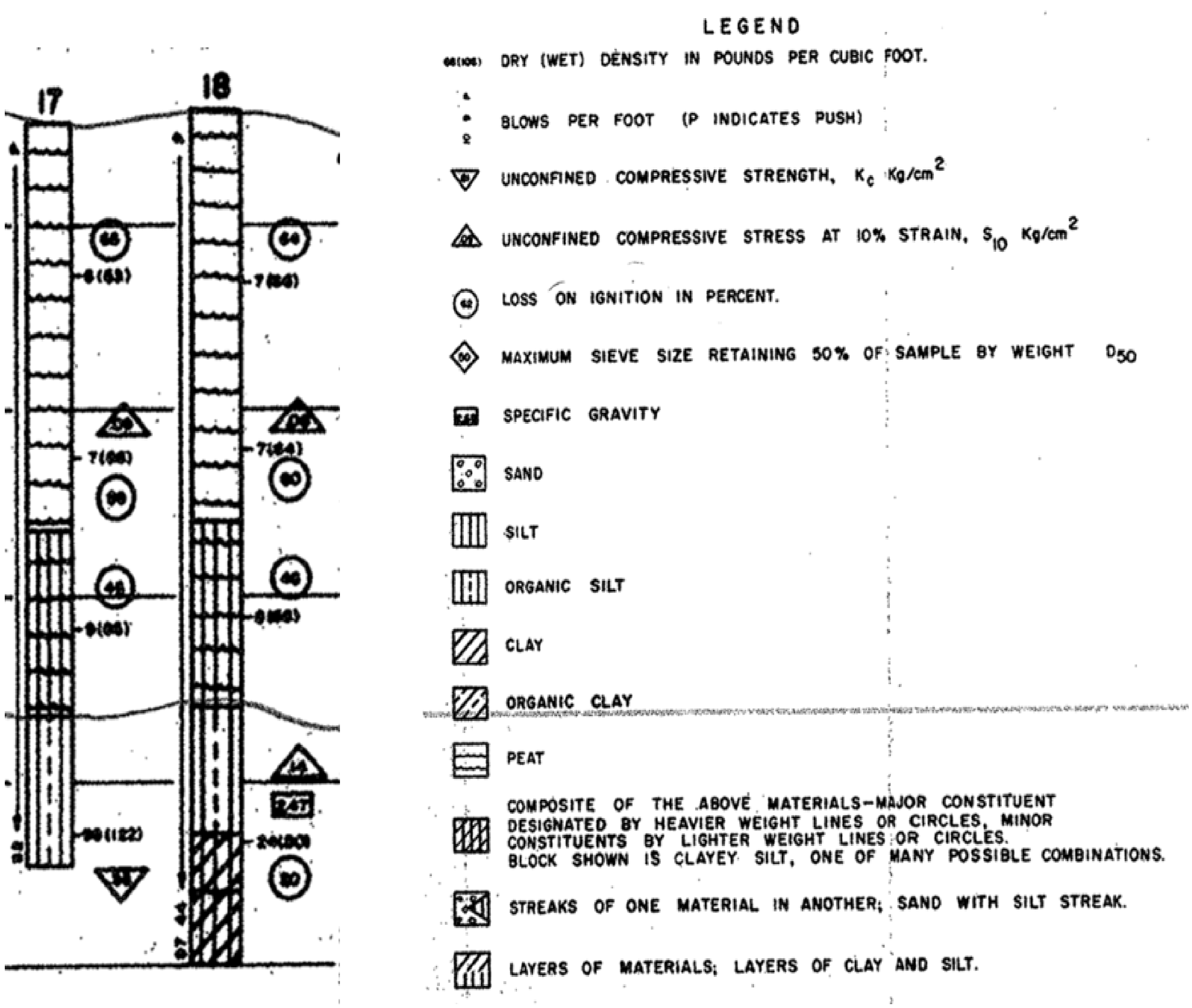

Borehole logs were obtained from two sources, a DWR borehole database and the McDonald Island GIS Portal,[3] maintained by Kjeldsen, Sinnock and Neudeck, Inc., a civil engineering firm.

[3] https://www.arcgis.com/apps/MapSeries/index.html?appid=37d32f49745945eaa188dd212594fe7b#

Site 1 — North

Site 1 is located at the north end of the island, where Whiskey Slough intersects the north edge of the island. A seismic survey 300 meters long was recorded between adjacent DWR 10,000-foot markers 350+00 and 360+00 (Figure 9). At least six boreholes exist at this location; four were drilled in 2011 and two were drilled in 1958 (Figure 10). Two of the 2011 logs are incomplete; accordingly, the research team had only the first page of the logs. Nonetheless, the combined data from the 2011 and the 1958 logs indicate that a layer of peat or fat clay at least 10 feet thick lies beneath the levee.

Figure 9: Map of Site 1, North Side of Island, Showing the Extent of the Seismic Survey

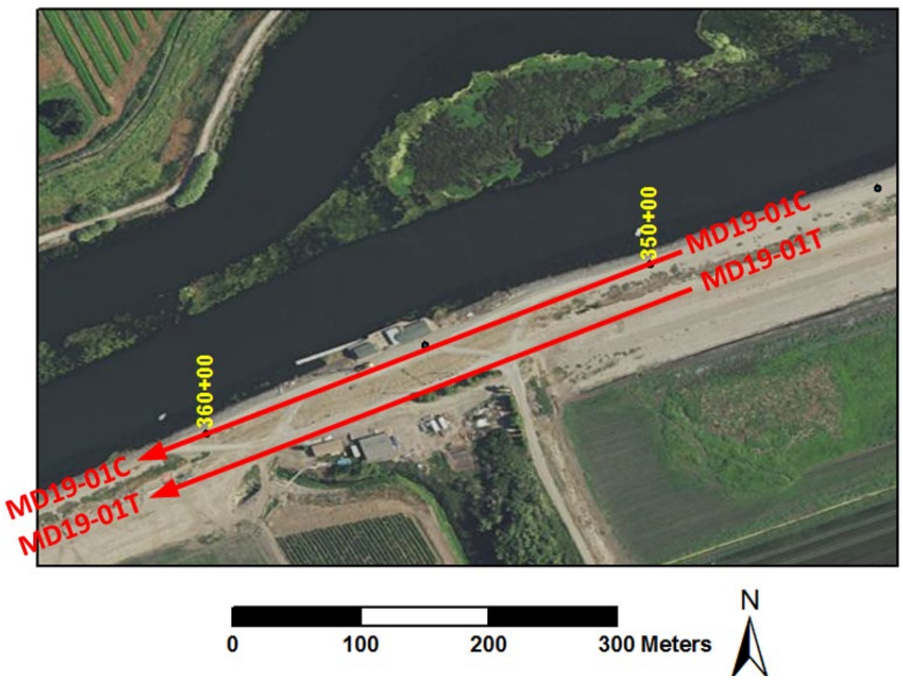

Figure 10: Basemap Showing Locations of Four Boreholes at Site 1 (North): 1-B1, 1-B2, 1-B3, and 1-B4

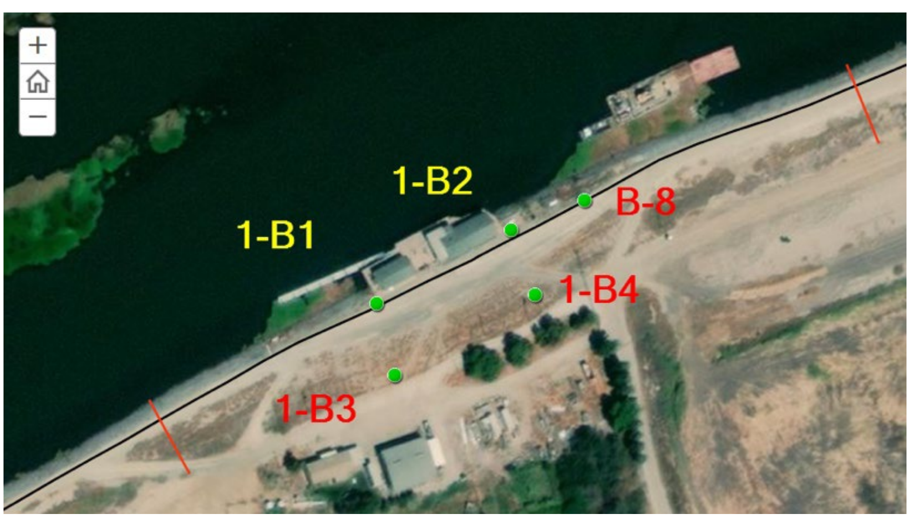

Remote Sensing

The research team jointly used the airborne and spaceborne SAR data, the SRTM digital elevation dataset, and the LiDAR DEM to evaluate the stability of the Delta and its levee system. The research team used Sentinel-1 satellite ascending track #35 SAR data spanning 2014-2018 to estimate the vertical displacements over the delta. Although the coherence was not promising due to the relatively shorter C-band wavelength (5.5 centimeters [cm]) and the delta wetland covers, the average displacements were still resolvable through time-series stacking. Due to the high temporal sampling rate (6/12 days) of the Sentinel-1A/B mission, the spatially randomly behaved atmospheric artifacts can be canceled out via a strategy of small temporal subsets. Note that the InSAR-derived displacements are not in a geodetic reference frame, and they are relative motions with respect to a stable area within the scene.

The research team used the urban area west of the main delta system (white star in Figure 11) as the reference. It is worth mentioning that the InSAR method measures the motions' projection on the slant range, which is mainly vertical and also contains a small fraction from the east-west direction. Satellite InSAR observations are not sensitive to the north-south motions (if any) due to the polar orbiting trajectory. The research team then translated the slant range measurements into the vertical dimension based on the trigonometric relationship.

The research team focused on the deformation on two scales: extensive areas of subsidence that may be vulnerable to flooding, and localized segments with high displacement gradients that suggest slope instability. Figure 11 shows the preliminary results of the vertical displacements along the levees. Results may be biased by the absolute motion of the reference area, the long-wavelength tectonic signals, phase changes resulting from the soil moisture changes, unwrapping errors, etc. The white star is the reference area. Black lines are the tectonic faults in which the dashed lines are the unconfirmed faults.

Overall, the southern parts toward the San Joaquin Valley show more subsidence (up to 60 mm/yr within the extent of the study area), consistent with previous NASA/UAVSAR results (Bekaert et al., 2019). The widespread land subsidence due to groundwater withdrawal over the valley has been problematic since the mid-1920s and may affect the integrity of levee systems. The area of interest — the McDonald Tract — is relatively stable, without high displacement gradients, and the subsidence rates are gradually increasing toward the south. In good agreement with the 2009-2015 InSAR results from the airborne NASA/UAVSAR system, the southwest corner of Sherman Island underwent relatively rapid subsidence (Deverel et al., 2016; NASA, 2017). More attention needs to be paid to the levee segments with high displacement gradients.

UAVSAR results highlighted the subsidence of Sherman Island in the westernmost section of the Delta, which stands between the saline ocean water from the San Francisco Bay and the rest of the Delta (Deverel et al., 2016; NASA, 2017). Sherman Island subsided 13 mm/yr ± 2 mm/yr during 2009-2014 (Sharma et al., 2016), and the peak subsidence rate was as high as 160 mm/yr ± 4.4 mm/yr during 2009-2015 (Bekaert et al., 2019). On average, the Delta is subsiding at a rate of 9.2 mm/yr ± 4.4 mm/yr (Bekaert et al., 2019).

Processed Sentinel-1 data shows the relative subsidence velocity of McDonald Island relative to that of the urban area west of the main delta system. The preliminary measurements were made along the line-of-sight direction of the Sentinel-1 ascending track #35.

Figure 11: Preliminary Results of the Vertical Subsidence of the Delta Levees

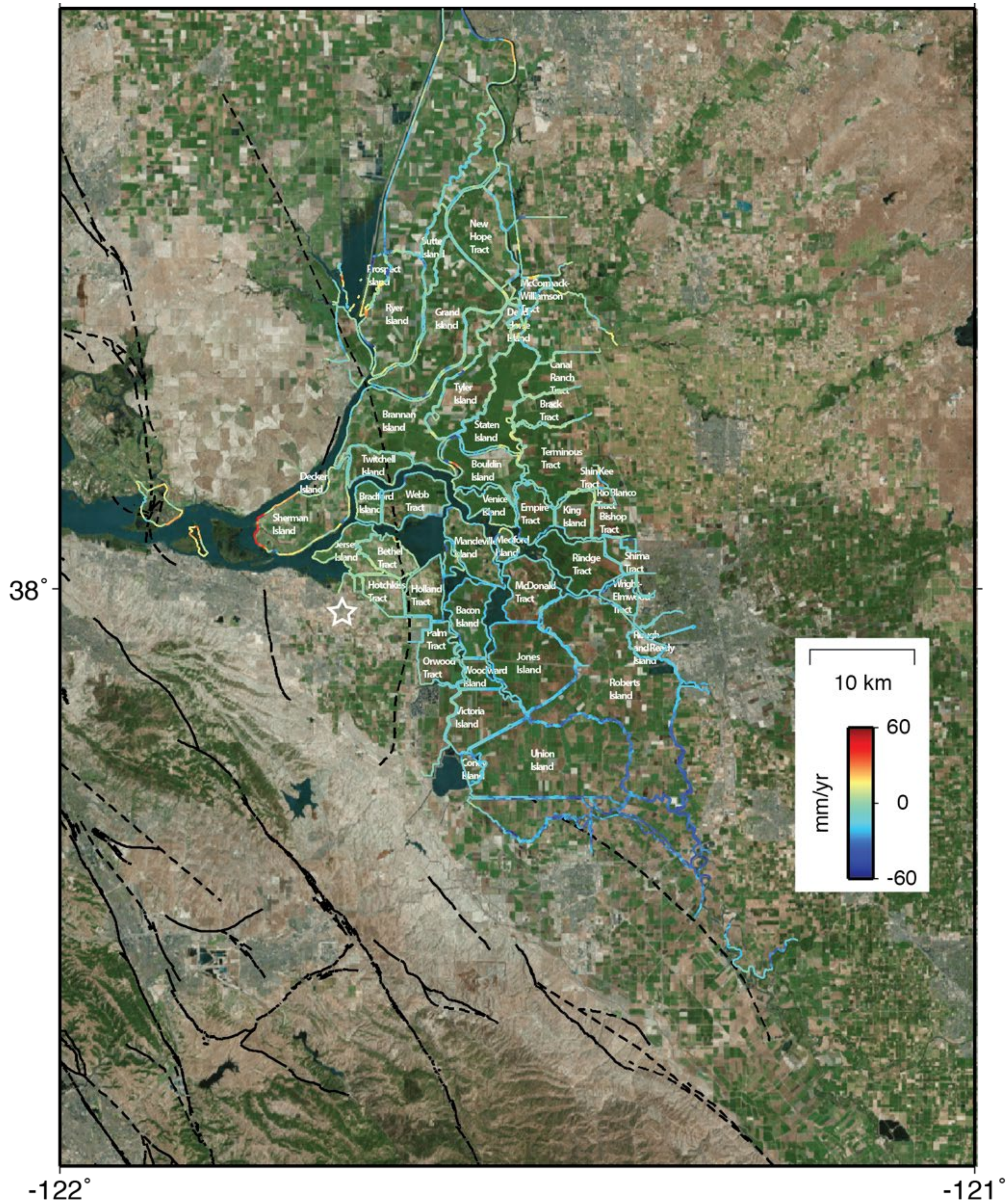

The study focused on the levees along McDonald Island. The high gradients in the displacement map (Figure 12) are shown on the left (where color changes), and the high amplitude dispersions are shown on the right (the reddish targets); the latter identify the suspicious segments that may be associated with land cover changes or instability.

Figure 12: Preliminary Results From InSAR Analysis for McDonald Island and Its Vicinity (From July 2019)

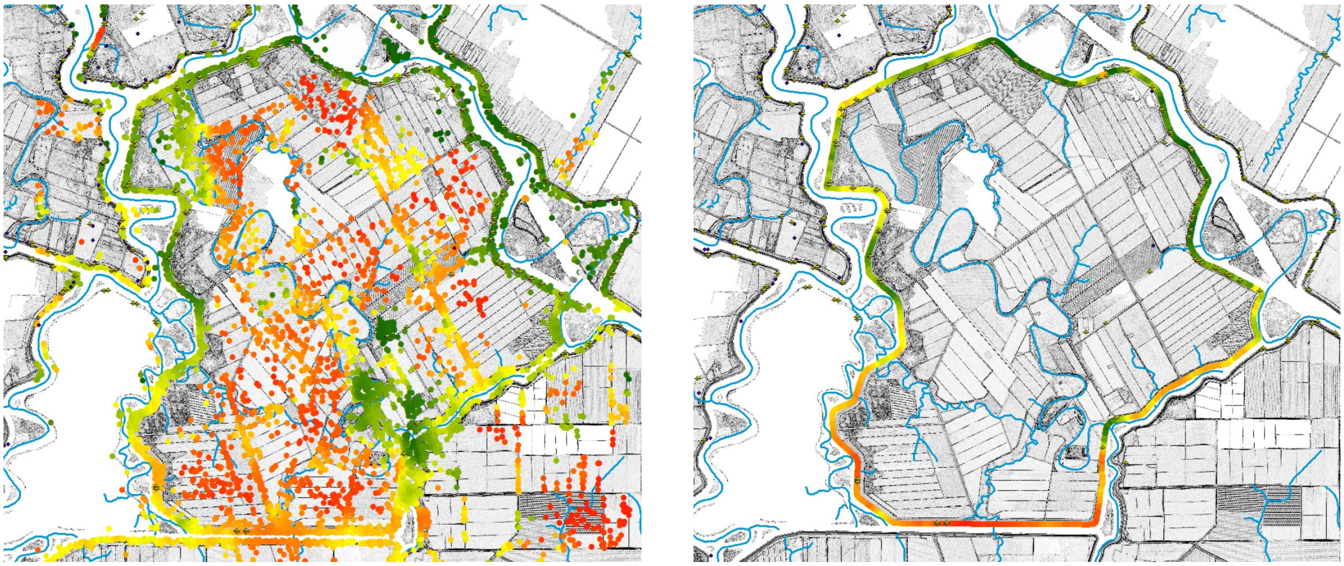

(Left) Vertical velocity of surface elevation changes for McDonald Island. (Right) Vertical velocity of surface elevation changes specific to McDonald Island levees. Red indicates relatively high velocity and green indicates relatively low velocity.

Differential DEM Analysis

The research team compared the DEM difference between the 30-m-posting 2000 SRTM DEM and the 0.3-m-posting 2018 LiDAR DEM after resampling (Figure 13). An elevation increase of greater than (>) 4m was found at a newly upgraded building in the southeastern part of the island. Here the research team highlighted three levee segments covered by the 2018 LiDAR DEM. The southeastern segment showed elevation increase while the two segments in the southwestern part showed elevation decrease. This qualitative comparison was affected by uncertainties due to coarse SRTM resolution and the applied different electromagnetic wavelengths (and thus penetration depth) of the two DEM sources.

Figure 13: 2000 SRTM DEM Versus 2018 LiDAR DEM

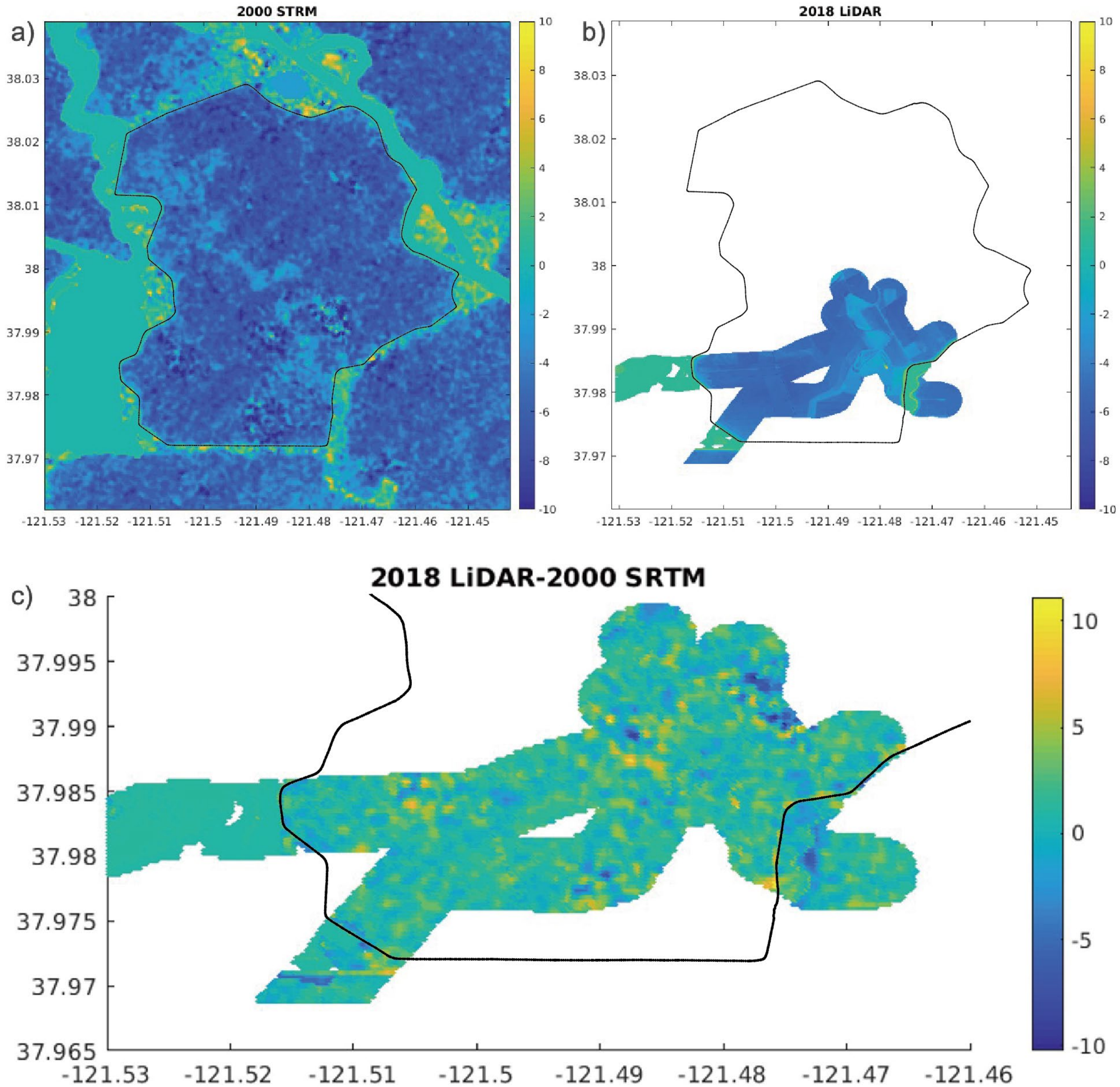

Geophysical Surveys

Geophysical field work was conducted at three sites on McDonald Island (Figure 1). Sites were selected after review of topo quads, soil maps, air photos, InSAR data, and the availability of borehole logs. Site 1 is located where a natural channel intersects the perimeter levee (north end of Whiskey Slough), Site 2 is at the south end of the island where preliminary InSAR data indicate that the levee is subsiding, and Site 3 is on the northeast side of the island in an area that appears to be relatively stable.

Seismic surveys were carried out along both the top and the bottom of the perimeter levee using the surface wave method. More specifically, the research team used the 2D MASW method. Seismic surveys were performed using a land streamer to obtain Vs estimates within the levee body and beneath the levee. Of the different geophysical methods used in this study, the seismic method was the most time and labor intensive; however, it provided an essential indicator of levee integrity, the Vs.

Surveys included active-source seismic, passive seismic, electrical resistivity, and GPR. Active-source seismic surveys were conducted along the crown of the levee using a 24-channel land streamer and sledgehammer source (Table 1). Passive seismic was recorded along the levee toe using nodal (cableless) seismographs. A total of six seismic profiles were recorded, three active and three passive. Four profiles were 300m long and two were 200m long. An example profile of seismic Vs from the passive survey is shown in Figure 14.

Table 1: Summary of Data Products from Geophysical Surveys at McDonald Island

Method	Site	Crown or Toe	Length (m)
Active seismic	1. Whiskey	Crown	300
Active seismic	2. South	Crown	200
Active seismic	3. Spud	Crown	300
Passive seismic	1. Whiskey	Toe	300
Passive seismic	2. South	Toe	300
Passive seismic	3. Spud	Toe	300
Resistivity	1. Whiskey	Crown	500
Resistivity	1. Whiskey	Toe	500
Resistivity	2. South	Crown	1000
Resistivity	2. South	Toe	400
Resistivity	3. Spud	Crown	650
Resistivity	3. Spud	Toe	650
GPR	1. Whiskey	Crown	300
GPR	1. Whiskey	Toe	300
GPR	2. South	Crown	300
GPR	3. Spud	Crown	300
GPR	3. Spud	Toe	300

The main data product for each site is a 2D seismic Vs section prepared by combining data from active and passive surveys. New velocity models 15m deep with a smaller layer thickness than previous models were prepared for all three sites to capture near-surface details of the velocity model; these are important for characterizing the levee and the materials immediately beneath it. An example of the velocity model for site 1 is shown in Figure 14.

Figure 14: Shear wave Velocity (Vs) Profile, Site 1

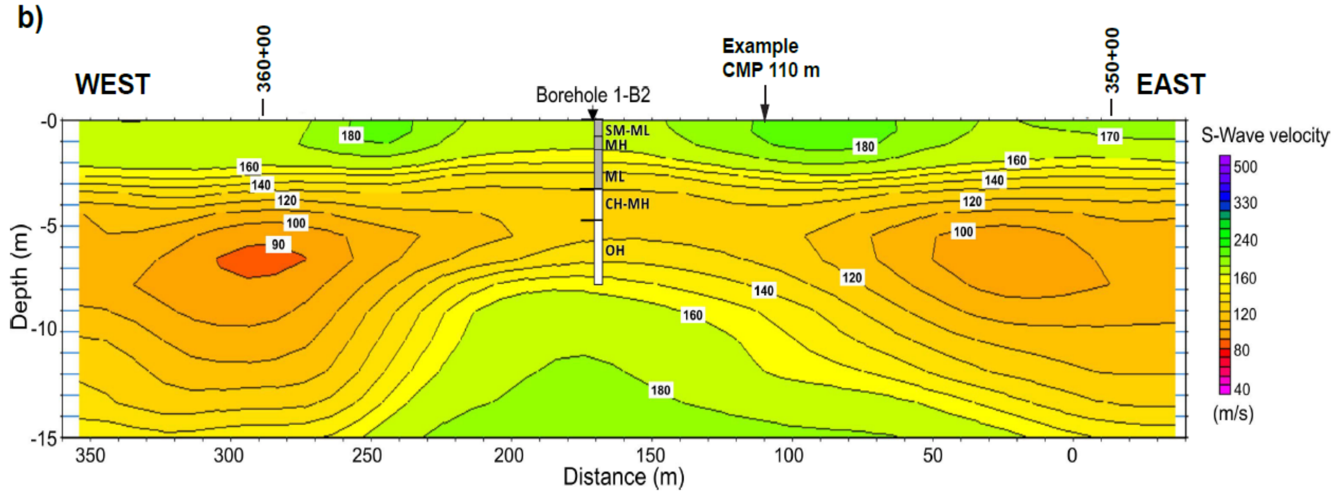

Distance posts are DWR 1000-foot markers. Data are from combined active and passive surveys. Higher-velocity material in the uppermost 3 meters corresponds to levee fill material. Velocity decreases sharply at a depth of approximately (~) 3m. The borehole log 1-B2 at Site 1 (North), drilled in 2011, shows 3.2-m-thick levee fill material (gray section of the borehole) composed of silty sand (SM) and silt with sand (ML); this is underlain by fat clay/elastic silt (CH/MH), followed by organic clay (OH) (ENGEO Inc., 2011).

There is a velocity reversal (a decrease in velocity with depth) at depths that correspond roughly to the base of the levee at Site 2, which appears to be experiencing subsidence. The low-velocity zone at this site is thinner and more laterally continuous than the one at Site 1. The low-velocity zone at this site is centered at a depth of 4m, and velocities range from about 80 to 120 m/s. This low velocity zone appears to correspond to a peat layer beneath the levee body.

Electrical resistivity was recorded along both the crown and the toe of the levee at each of the three sites using an OhmMapper[4] 4-receiver CCD system. Six profiles were recorded. Profile lengths were 400m (1 profile), 500m (2 profiles), 600m (2 profiles), and 1000m (1 profile). The resistivity profiles extended beyond the lengths of the seismic profiles in nearly all cases to reach locations where additional borehole logs were available. A 1000-m-long resistivity profile was recorded along the crown at one site to investigate a portion of the levee with apparent differential settling (Figure 15 and Figure 16).

GPR profiles were recorded along the crown of the levee at all three sites and along the toe of the levee at two sites, for a total of five profiles, each 300m in length.

[4] The Geometrics OhmMapper is a capacitively-coupled resistivity meter that measures the electrical properties of rock and soil without cumbersome galvanic electrodes used in traditional resistivity surveys. https://geometrics.com/wp-content/uploads/2018/10/OhmMapper_Spec_Sheet.pdf

Figure 15: Location of Passive Seismic Survey at Site 1, North End of Whiskey Slough

Figure 16: Shear-wave Velocity Profile From Passive Seismic Survey at Site 1

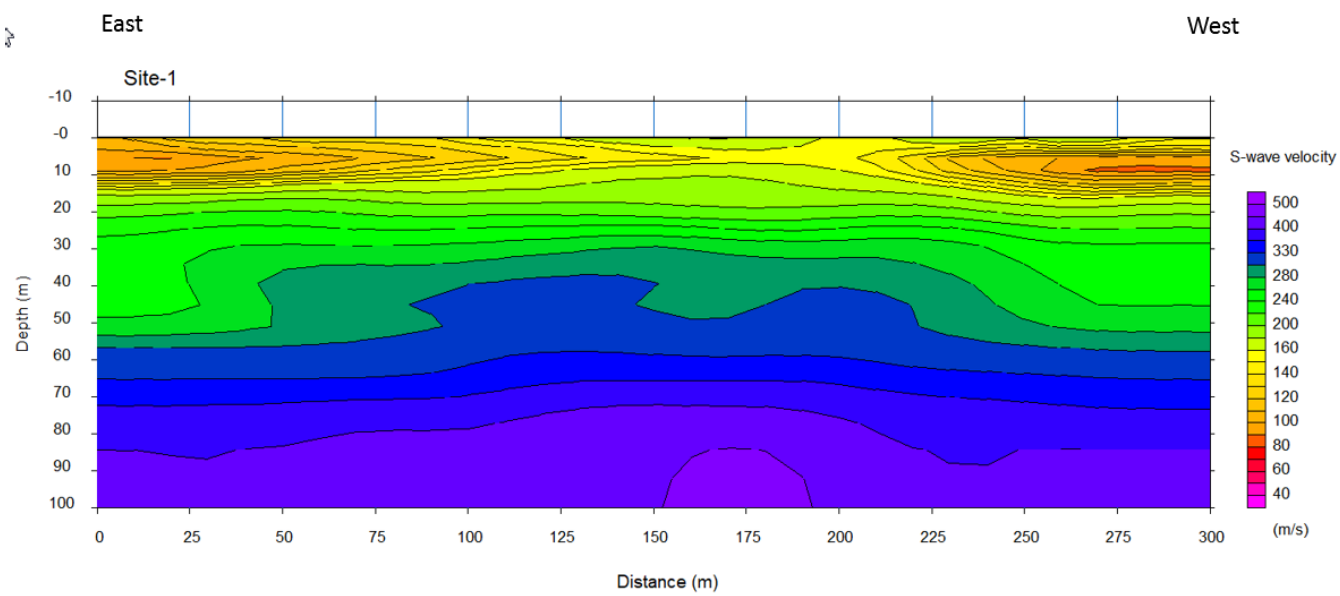

A new survey site was added at the site of a 1982 levee breach, which occurred on the northwest side of the island. The location of the breach was indicated by the landowner. The top of the levee was surveyed with a single line 1060m long, 574A. The base of the levee was surveyed with three shorter lines; 527B, 525B, and 525A. Data quality at this location was variable due to wind noise, but nearly all data were usable.

A portion of the line centered at the 1982 breach is shown in Figure 17. The breach appears to be ~100m wide. The full depth of the breach appears to be 8m to 10m below the levee surface. The area of the breach shows anomalously high velocities. Velocities exceed 200m/s (green color) and evidently reflect the presence of repair materials (rock) instead of the low-velocity peat (orange color) on either side of the breach.

Figure 17: Seismic Velocity Profile at Site 2 (South), Depth Scale to 60 Meters

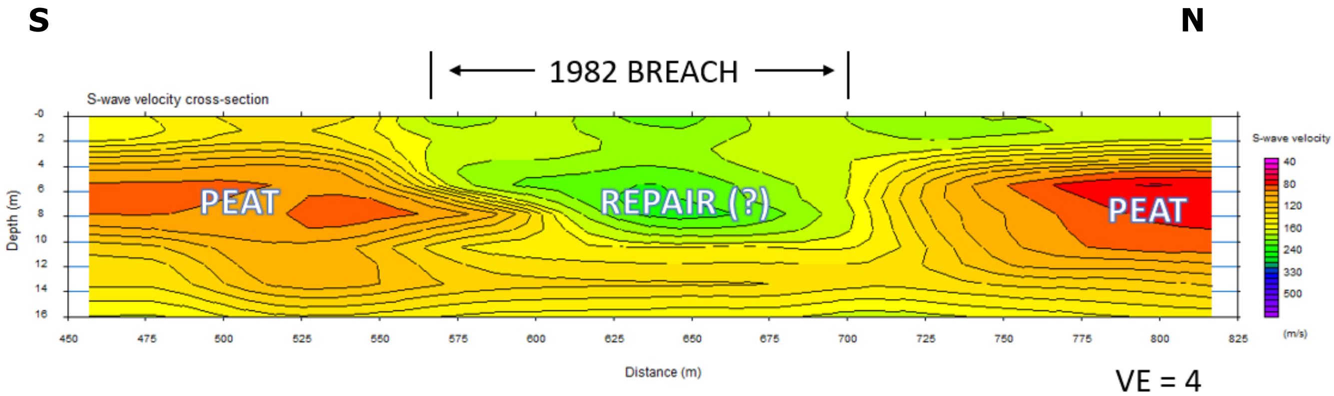

Electrical Resistivity Surveys

Electrical resistivity surveys were recorded along both the crown and the toe of the levee at each of three sites during both the 2019 surveys and the 2022 surveys. The examples shown in Figure 18 and Figure 19 are from the 2019 surveys. The first site is located at the north edge of McDonald Island, where a tidal channel intersects the edge of the island. The second site is located along the southern edge of the island in a location that was identified as having a high subsidence rate based on InSAR data. The third site is on the eastern side of the island in an area that is believed to be stable based on InSAR data.

A new survey site was added in the 2022 surveys at the site of a 1982 levee breach, which occurred on the northwest side of the island. The location of the breach was indicated by the landowner. The top of the levee was surveyed with a single line 1060m long, 574A. The base of the levee was surveyed with three shorter lines; 527B, 525B, and 525A. Data quality at this location was variable due to wind noise, but nearly all data were usable.

Figure 18: Site 2, Showing Extent of Electrical Resistivity Profiles

The toe profile (magenta) is 400m long; the crown profile (green) is 1000m long.

Figure 19: Resistivity Profiles From Site 2

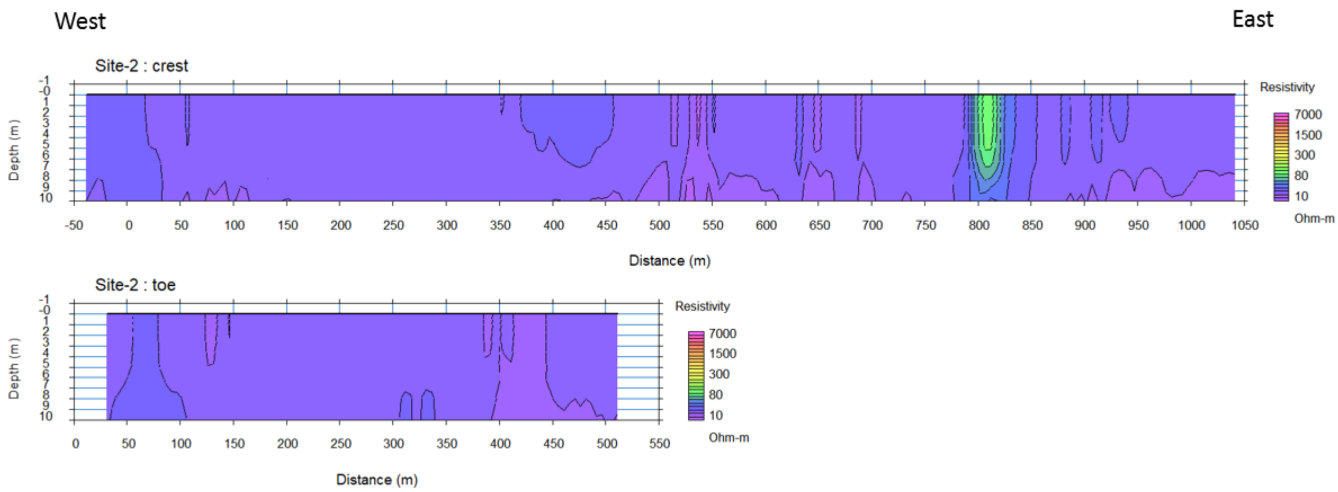

GPR Surveys

GPR surveys were carried out at three sites on McDonald Island in 2019 (Figure 1). The GPR profiles were 300m long, recorded along the crown and the toe of the levee at each of the three sites, except at Site 2 where a toe line was not completed due to equipment problems. The GPR surveys coincide with locations where seismic and electrical resistivity surveys were recorded. GPR data were recorded using 100-megahertz (MHz) antennas and a step size of 1 m. Sample profiles are shown in Figure 20.

Figure 20: Ground Penetrating Radar Profile, Site 3 (East Side of McDonald Island, Across From Spud Island), Along Levee Toe

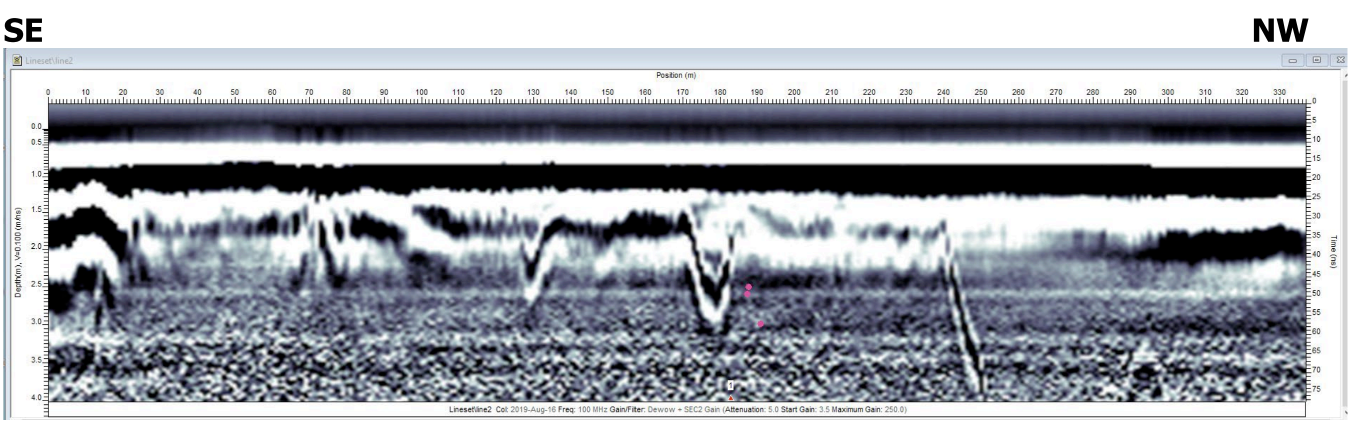

Levee Stability Assessments

A goal for the project was to incorporate geophysical measurements into stability assessments for levees (Figures 21 and 22). The geophysical measurements were anticipated to identify spatial distributions of soil properties, and the spatial distribution of soil properties must be represented in the stability analyses to properly capture the levee response.

An efficient algorithm for generating spatially correlated random field realizations was developed. Specifically, Cholesky decomposition was performed on a coarser set of grid points, with interpolate between the coarse grid points using Kriging.[5] This approach is significantly less computationally expensive, but it is associated with errors that must be quantified and controlled.

Figure 21: Shear Wave Velocity Profile from Crest of Levee Cross-section at Boring Log Mcd-tra-24

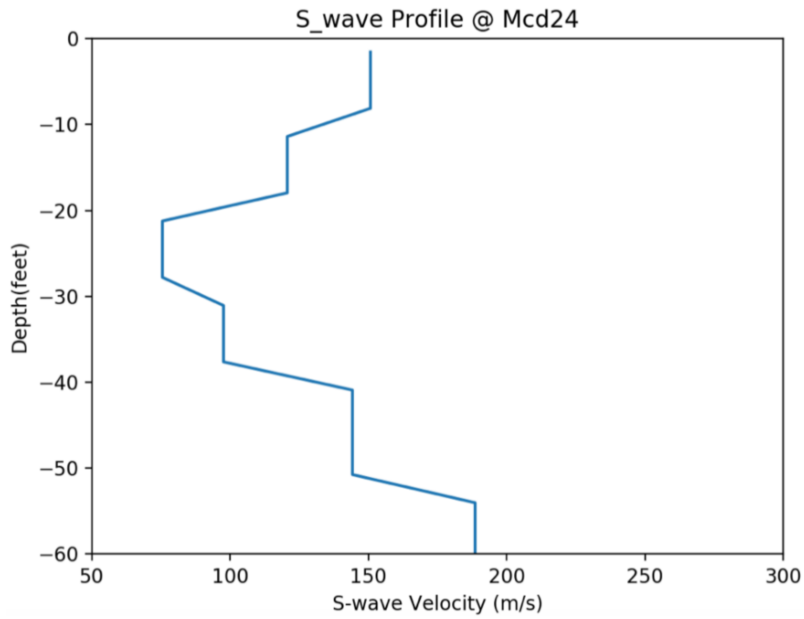

Figure 22: Levee Cross-section Example With Soil Layer Defined (Sketch)

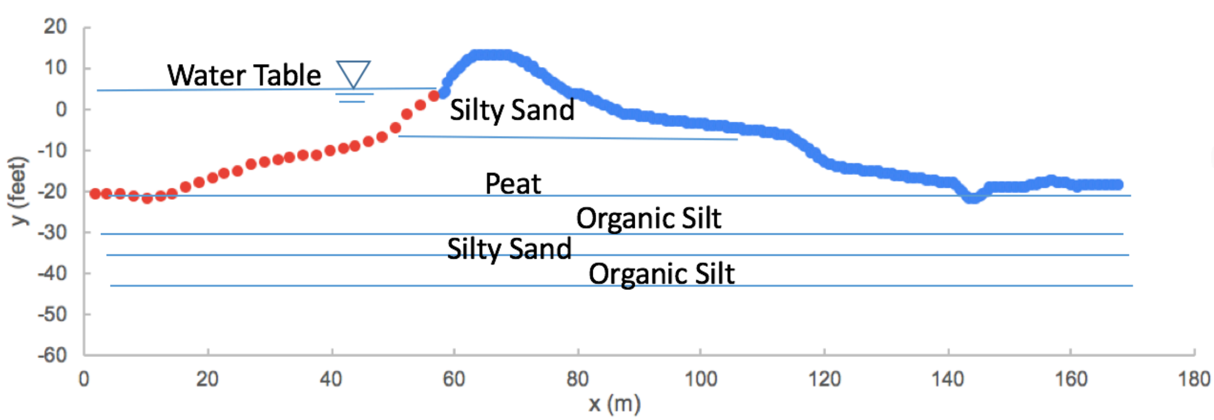

By using a profile such as that shown in Figure 22, the research team moved forward to build up a finite element model and run simulations in OpenSees. However, the research team found it necessary and useful to first run a steady state seepage analysis in RS2[6] to get the

[5] Kriging predicts the value of a function at a given point by computing a weighted average of the known values of the function in the neighborhood of the point.

[6] A software program that Analyzes slopes, foundations, tunnels, and more using the shear strength reduction method for accurate stability assessments. https://www.rocscience.com/software/rs2.

phreatic surface, which is quite important in the subsequent mesh generation and finite element simulations. RS2 is software for analyzing the shear strength of slopes, foundations, tunnels, and more. Figure 23 shows the finite element model that was built up in RS2 as the boundary conditions, and the water table was indicated in the figure as well. Figure 24 shows the pore water pressure distribution within the levee model after seepage.

Figure 23: Finite Element Model in RS2 to Run Seepage Analysis

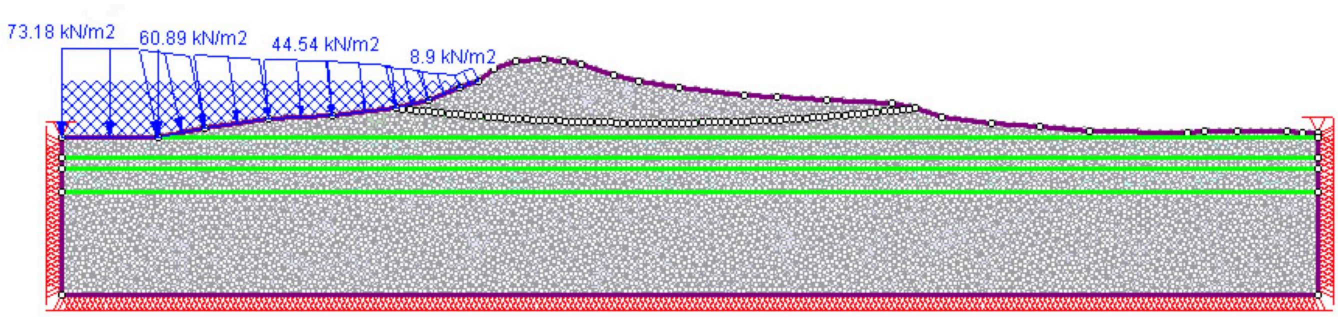

Figure 24: Pore Water Pressure Distribution After Seepage Analysis

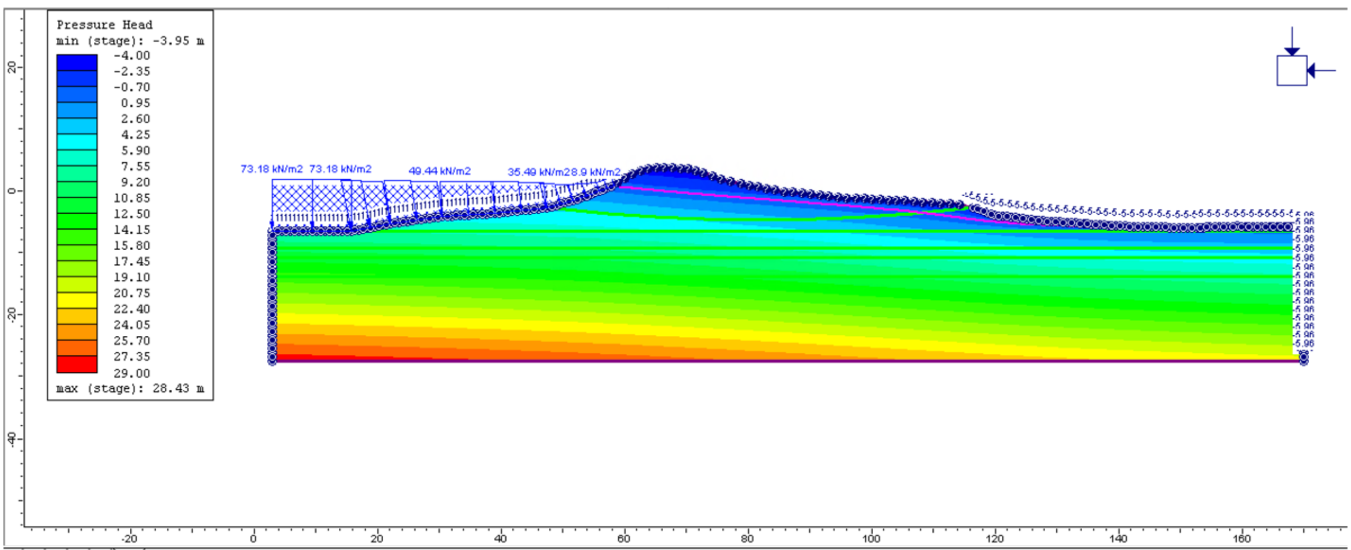

The next step was to run the dynamic simulation in OpenSees. The research team used the shear strength reduction method in RS2, which provides a critical strength reduction factor. By varying the horizontal correlation length, the research team was able to look into how the levee deforms and fails differently and how the strength reduction factor changes. For example, when the horizontal correlation length is 1m, the factor of safety is 1.85, as shown in Figure 25.

Figure 25: Finite Element Simulation Using Strength Reduction Method for a Levee with Spatial Correlation Length of Undrained Shear Strength Equal to 1.0m

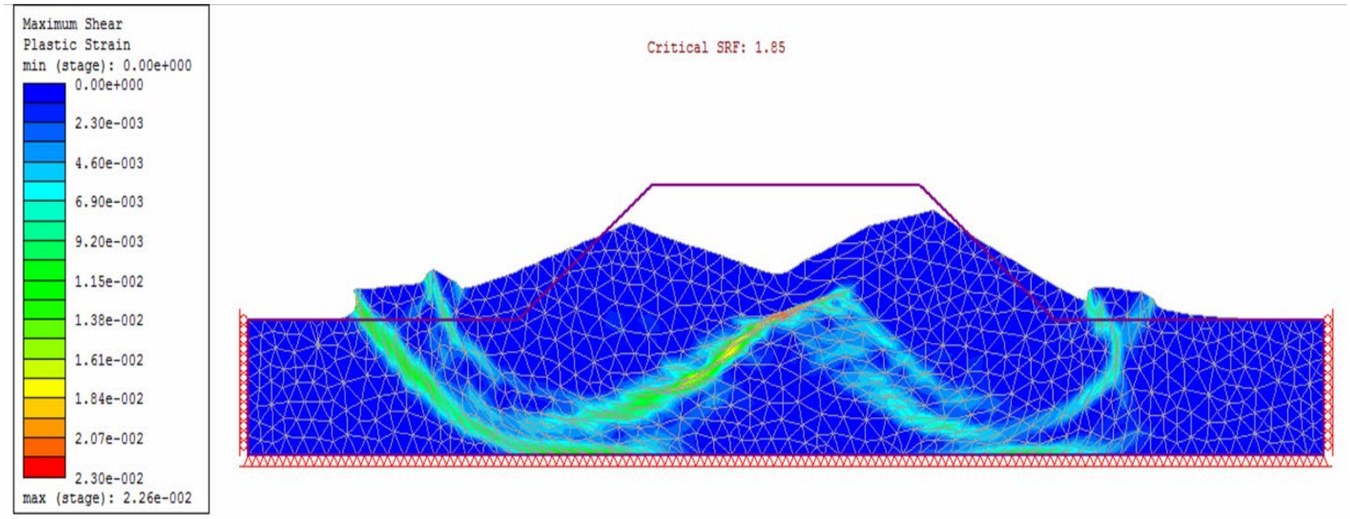

CHAPTER 4: Conclusion

Remote Sensing

The results of this study demonstrate that regional deformation measurement in an urban environment can be achieved by InSAR methods at a high accuracy of a few mm/yr when a large collection of SAR images is available. A suggested temporal threshold for C-band spaceborne Sentinel-1 data is less than one month, to maintain the coherence in the Delta.

A regional displacement pattern over the Delta has been quantified, highlighted by an increasing subsidence to the south, where groundwater depletion occurs in the San Joaquin Valley. However, resolving localized deformation in the delta environment remains challenging due to constantly changing soil moistures, vegetated covers from harvest and seasonal growth, and atmospheric turbulence.

As a complement, InSAR coherence and SAR amplitude can be used to unveil land cover changes and soil-moisture-related processes. The change of amplitude dispersion shows two linear features southwest of McDonald Island that were interpreted to be due to road widening. Repeated harvests can be effectively located and traced as well. A joint use of optical and microwave remote sensing images from the ground, air, and space and a dense monitoring network of in-situ geophysical and geotechnical tools can help better understand the spatiotemporal development of the levee systems.

After completing these updates and modifications on finite element models of the Bacon Island levee (see Appendix C), the research team believes new models can yield more accurate and reliable results of levee seismic fragility functions.

Applicability of Geophysical Techniques

For carrying out geophysical surveys at locations where the levee curves or bends at a sharp corner of an island, towed systems are not practical, and a different data acquisition strategy is needed. For seismic surveying, either a cabled system or a nodal system with fixed geophones is preferred to a land streamer. For electrical resistivity surveying, a system with planted electrodes (galvanic system) is preferred to a towed CCD system. In cases where the recording geometry deviates significantly from a straight line, data processing must take into account the nonlinear recording geometry.

One of the findings is that the horizontal variability of the levee, as indicated by seismic Vs is much more rapid in the levee body (upper 3 meters) than in the geologic substrate.

Implications for Levee Risk Evaluation

A key result of this study is that geophysical measurements can be used to identify spatial distributions of soil properties in levees, which can be used for stability analyses to properly capture the levee response to seismic events.

An efficient algorithm for generating spatially correlated random field realizations was developed for this project incorporating Cholesky decomposition, with interpolation between grid points using Kriging.

GLOSSARY AND LIST OF ACRONYMS

Term	Definition
$(S_u/\sigma_v')_{nc}$	shear strength ratio
~	approximately
>	greater than
1D	one-dimensional
2D MASW	two-dimensional multichannel analysis of surface waves
CCD	capacitively-coupled dipole
CEC	California Energy Commission
CH/MH	fat clay/elastic silt
cm	centimeter
CMP	common midpoint
CMP-CC	common midpoint cross correlation
CMP-SPAC	common midpoint spatial autocorrelation
CO_2	carbon dioxide
CPT	cone penetration tests
DA	dispersion of amplitude
dB	decibel
Delta	Sacramento-San Joaquin Delta
DEM	digital elevation model
DWR	Department of Water Resources
GIS	geographical information system
G_{MAX}	small-strain shear modulus
GPR	ground penetrating radar
GPS	global positioning system
Hz	hertz
InSAR	interferometric synthetic aperture radar
kg	kilogram
km	kilometer
km^2	kilometers squared
kPa	kilopascals
LIDAR	laser imaging, detection, and ranging
LOS	line-of-sight

Term	Definition
m	meter
m/s	meter per second
MHz	megahertz
ML	silt with sand
mm/yr	millimeters per year
MRD	modulus reduction and damping
NASA/JPL	National Aeronautics and Space Administration Jet Propulsion Laboratory
N_{kt}	cone factor
OH	organic clay
psf	per square foot
SAR	synthetic aperture radar
SLC	single look complex
SM	silty sand
SPT	standard penetration test
SRTM	Shuttle Radar Topography Mission
TCU	triaxial consolidation undrained
TUU	triaxial unconsolidated undrained
UAVSAR	uninhabited aerial vehicle synthetic aperture radar
USDA	United States Department of Agriculture
USGS	United States Geological Survey
VE	vertical exaggeration
Vs	shear wave velocity

References

An, K., C. Jones, D. Bekaert, and V. Bennett. 2020 (March). "Radar interferometry offers new monitoring approach for critical flood control infrastructure." *Authorea*. DOI:10.1002/essoar.10502490.1

Bekaert, D.P.S., C.E. Jones, K. An, and M.-H. Huang. 2019. "Exploiting UAVSAR for a comprehensive analysis of subsidence in the Sacramento Delta." *Remote Sensing of Environment.* January. 220, 124–134. DOI:10.1016/j.rse.2018.10.023

Brooks, B.A., G. Bawden, D. Manjunath, C. Werner, N. Knowles, J. Foster, J. Dudas, and D.R. Cayan. 2012. "Contemporaneous Subsidence and Levee Overtopping Potential, Sacramento-San Joaquin Delta, California." *San Francisco Estuary and Watershed Science*. 10 (1). Available at https://www.semanticscholar.org/paper/Contemporaneous-Subsidence-and-Levee-Overtopping-Brooks-Bawden/88a3d7bca4b33bafa546a5d16cdb8ceb0a30e6c6

Cohen, D.A., S. Deverel, L. A. Johnson. 1998. *Feasibility study of differential SAR interferometry for subsidence monitoring in the Sacramento-San Joaquin Delta*. IGARSS '98. Sensing and Managing the Environment. 1998 IEEE International Geoscience and Remote Sensing. Symposium Proceedings. (Cat. No.98CH36174). Feasibility study of differential SAR interferometry for subsidence monitoring

Craig, M., K. Hayashi, and S. Shuler. 2015. *Improvements to the Near Surface Velocity Model of the Sacramento-San Joaquin Delta*. Final Technical Report, USGS Award Number G14AP00098

Darendeli, M.B. 2001. "Development of a new family of normalized modulus reduction and material damping curves." Ph.D. dissertation. The University of Texas at Austin. Available at https://repositories.lib.utexas.edu/items/efea68dd-895b-4f28-ac6e-71872ca5291a

Deverel, S.J., S. Bachand, S.J. Brandenberg, C.E. Jones, J.P. Stewart, and P. Zimmaro. 2016. "Factors and processes affecting delta levee system vulnerability." *San Francisco Estuary and Watershed Science*. 14 (4). Available at https://www.semanticscholar.org/paper/Factors-and-Processes-Affecting-Delta-Levee-System-Deverel-Bachand/b8eae65c28a4beb2700538da570095bb80c5a7e8

ENGEO Inc. 2011. "Log of Boring 1-B2. Geotechnical Exploration, McDonald Island Setback Levee, San Joaquin County, CA." Courtesy KSN, McDonald Island GIS Portal, accessed 1 August 2020. Available at https://www.arcgis.com/apps/MapSeries/index.html?appid=37d32f49745945eaa188dd212594fe7b#

Gravely, M., and N. Smith. 2016. *Natural Gas Research and Development Program: Proposed Program Plan and Funding Request for Fiscal Year 2016-17*. California Energy Commission Research and Development Division. Publication Number: CEC-500-2016-063.

Available at https://www.energy.ca.gov/sites/default/files/2021-04/CEC-500-2016-063.pdf

Hardin, B.O., and V.P. Drnevich. 1972. "Shear modulus and damping in soils: design equations and curves." *Journal of the Soil Mechanics and Foundations Division*. 98 (7), 667-692. Available at http://dx.doi.org/10.1061/JSFEAQ.0001760

Ingebritsen, S., M. Ikehara, D. Galloway, and D. Jones. 2000. "Delta subsidence in California: the sinking heart of the state." U.S. Geological Survey, Fact Sheet 005-00. Available at https://pubs.usgs.gov/fs/2000/fs00500/

Jones, C.E., J. Dudas, and G.W. Bawden. 2016. "Application of Remote Sensing to Assessment of Water Conveyance Infrastructure Integrity." In R.L. Anderson and H. Ferriz (eds.), *Applied Geology in California*. Special Publication 26, 253–271. Association of Environmental Engineering Geologists. Star Publishing Company

Jongejan R.B., and B. Maaskant. 2015. "Quantifying Flood Risks in the Netherlands." *Risk Analysis: An International Journal*. 35, 252–264. Society for Risk Analysis. Available at https://doi.org/10.1111/risa.12285

Ladd, C.C., and R. Foott. 1974. "New design procedure for stability of soft clays." *Journal of the Geotechnical Engineering Division*. 100 (7), 763-786. Available at https://doi.org/10.1061/AJGEB6.0000066

Menq, F.Y. 2003. "Dynamic properties of sandy and gravelly soils." The University of Texas at Austin. Available at https://repositories.lib.utexas.edu/items/2a7a8fec-45f1-4c81-920d-b1af79679e2e

NASA. 2017. "Levees and Dams: Flood Defense for U.S. Communities." NISAR: The NASA-ISRO SAR Mission. Available at https://nisar.jpl.nasa.gov/documents/22/NISAR_Applications_Levees_and_Dams1.pdf

Seed, H.B., and U.-M. Idriss. 1970. "Soil moduli and damping factors for dynamic response analysis." *Journal of Terramechanics*. 8 (3). Available at https://ntrl.ntis.gov/NTRL/dashboard/searchResults/titleDetail/PB197869.xhtml

Sharma, P., C.E. Jones, J. Dudas, G.W. Bawden, and S. Deverel. 2016. "Monitoring of subsidence with UAVSAR on Sherman Island in California's Sacramento–San Joaquin Delta." *Remote Sensing of Environment*. 181, 218–236. Available at https://doi.org/10.1016/j.rse.2016.04.012

U.S. Geological Survey. 2013. "USGS Science at Work in the San Francisco Bay and Sacramento-San Joaquin Delta Estuary." Fact Sheet 2013–3037. Available at https://pubs.usgs.gov/fs/2013/3037/

Vrouwenvelder, T. 2006. "Spatial effects in reliability analysis of flood protection systems." International Forum on Engineering Decision Making, Second IFED Forum, April 26-29, Lake Louise, Canada. Available at http://www.taifu.dpri.kyoto-u.ac.jp/ifed/wp-content/uploads/sites/5/2015/04/vrouwenvelder_paper.pdf

Wang, L., T. Ishihara. 2022. New p-y model for seismic loading prediction of pile foundations in non-liquefiable and liquefiable soils considering modulus reduction and damping curves. *Soils and Foundations.* 62 (5). October, 101201.

Zimmaro, P., J.P. Stewart, S.J. Brandenberg, D.Y. Kwak, and R. Jongejan. 2019. "Multi-hazard system reliability of flood control levees." *Soil Dynamics and Earthquake Engineering* 124, 345-353. Available at https://doi.org/10.1016/j.soildyn.2018.04.043

Zwieback, S., S. Hensley, and I. Hajnsek. 2015. "Assessment of soil moisture effects on L-band radar interferometry." *Remote Sensing of Environment*. 164, 77–89. https://doi.org/10.1016/j.rse.2015.04.012

Project Deliverables

The Project Deliverables include the following:

Geophysical data.

Geotechnical analyses.

An article, "Active and passive seismic surface wave methods for levee assessment in the Sacramento-San Joaquin Delta, California, USA," published in the journal *Near Surface Geophysics* (2021, 19, 1), which describes the results of seismic surveys performed in 2019 for this project.

Project deliverables, including interim project reports, are available upon request by submitting an email to pubs@energy.ca.gov.

CALIFORNIA ENERGY COMMISSION

ENERGY RESEARCH AND DEVELOPMENT DIVISION

Appendix A: Remote Sensing Investigation on McDonald Island in the Sacramento-San Joaquin Delta

August 2024 | CEC-500-2024-093

APPENDIX A: Remote Sensing Investigation on McDonald Island in the Sacramento-San Joaquin Delta

Introduction

As an active remote sensing tool operating at microwave wavelength, Synthetic Aperture Radar (SAR) transmits electromagnetic waves to the ground and receives the echoes backscattered from the ground. The complex format radar signals can be interpreted as amplitude and phase. Amplitude mainly characterizes the physical properties of the ground objects, and phase is determined by the traveling distance of the electromagnetic waves. Spaceborne C-band ERS 1 & 2 (Cohen et al., 1998) and ENVISAT ASAR (Brooks et al., 2012) and airborne L-band UAVSAR data (Bekaert et al., 2019) have been used to study the Delta. The application of SAR interferometry (InSAR) in the Delta is challenged by phase decorrelation due to tidal marshes, wetlands, and reclaimed lands, especially when using relatively shorter-wavelength C-band data (Cohen et al., 1998; Brooks et al., 2012). For this non-urban landscape, L-band UAVSAR data have the advantage of longer-wavelength acquisitions, but the revisit time is on the timescale of months. UAVSAR results highlighted the subsidence of Sherman Island in the westernmost section of the Delta which stands between the saline ocean water from the San Francisco Bay and the rest of the Delta (Deverel et al. 2016; NASA, 2017). Sherman Island subsided at 13±2 mm/yr during 2009-2014 (Sharma et al., 2016), and the peak subsidence rate can reach as high as 160±4.4 mm/yr during 2009-2015 (Bekaert et al., 2019). On average, the Delta is subsiding at a rate of 9.2±4.4 mm/yr (Bekaert et al., 2019).

The research team jointly used the airborne and spaceborne SAR data, Shuttle Radar Topography Mission (SRTM) digital elevation model (DEM), and laser imaging, detection, and ranging (LiDAR) DEM to evaluate the stability of the Delta and its levee system. Table A-1 below provides general information and specifications of both the Sentinel-1 SAR and UAVSAR technology deployed for the evaluation.

Sentinel-1 SAR images

The C-band Copernicus satellite Sentinel-1A (wavelength: 5.6×10^{-2}m) was launched in 2014 by the European Space Agency, followed by the identical satellite Sentinel-1B in 2016. The temporal observation intervals of the Sentinel-1A/B satellites is 12 days, and 6-day pairs are sometimes available when Sentinel-1A and Sentinel-1B collect scenes over the same area during consecutive flyovers. The single-look pixel spacing in azimuth and range directions are 13.9m and 2.3m, respectively. The Sentinel-1 satellites have good orbital control, and the data are freely available. Therefore, Sentinel-1 becomes one of the most popular SAR data sources nowadays. Sentinel-1's ascending path 35 and descending path 42 cover the Delta. The image swath of the spaceborne Sentinel-1 mission stretches across about 250km to allow for regional mapping of radar phase and amplitude information.

UAVSAR SAR images

UAVSAR (Uninhabited Aerial Vehicle SAR) is operated by JPL/NASA. This L-band system (wavelength: 0.238m) has been repeatedly deployed over the Delta every half to two months. As an airborne imaging system, UAVSAR has small single-look pixel spacings of 0.6 and 1.67m in azimuth and range directions, respectively.

Three flight lines are available for McDonald Island. Flight lines #05524 and #23501 cover the entrance of the estuary, including the critical Sherman Island in the westernmost Delta. McDonald Island lies in the heart of the Delta and is mostly covered by an additional flight line #15503. The image swath is about 22km wide.

Table A-1: Remote Sensing Data

Mission	Agency	Wavelength (m)		Pixel spacing (m)		Path / Flight line	Number of scenes	Time window
				Azimuth	Range			
Sentinel-1	ESA Spaceborne	C	0.056	13.9	2.3	35 (asc.)	82	3/1/2015-8/6/2018
						42 (dec.)	137	12/02/2015-11/17/2019
UAVSAR	JPL/NASA Airborne	L	0.238	0.6	1.67	05524	39	11/19/2009-2/21/2019
						15503	64	07/18/2009-11/14/2017
						23501	16	2/18/2009-4/3/2017

Interferometric SAR (InSAR)

Interferometric SAR (InSAR) has been a widely used approach to measure ground displacements from phase difference between SAR acquisitions. After removing the topographic contribution simulated by an auxiliary DEM, the interferogram represents the displacement estimate using phase fringes. One fringe cycle corresponds to displacement along the radar line-of-sight (LOS; a.k.a., slant range) by half of the wavelength. To translate the interferogram into displacement measurements, phase fringes can be unwrapped referenced to a stable area (where little deformation is expected) and the consequent phase needs to be further multiplied with a coefficient related to the radar wavelength. As a quality indicator of the interferogram, coherence describes the signal stability. Under the assumption of ergodicity, coherence can be calculated by cross-correlating the patches between the reference and the secondary images. We applied 1 by 4 multilooks for Sentinel-1 data and 8 by 2 multilooks for UAVSAR data to enhance the signal-to-noise-ratio and thus coherence, at the cost of reduced spatial resolution. Note that JPL/NASA release stacks of coregistered single look complex (SLC) scenes for each UAVSAR flight line, and the InSAR computation can be directly performed on SLC stacks with the additional step of topographic phase removal.

The InSAR-derived displacements are not in any geodetic reference frame. They are relative motions with respect to an assumed stable area within the scene. Here we used an urban area west of the Delta (white star in Figure 1) as the reference. Results may be biased by the absolute motion of the reference area, the long-wavelength tectonic signals, phase changes resulting from soil moisture changes, unwrapping errors, and various sources of noise. Unfortunately, satellite InSAR observations are not sensitive to the north-south motions due to the polar orbiting trajectory. On the other hand, flight lines of the UAVSAR system can be oriented in any azimuth, Here we translated the LOS measurements into the vertical direction based on the angle of incidence and trigonometry.

Dispersion of amplitude (DA; a.k.a., amplitude dispersion) is the ratio between the standard deviation and the mean of time-series SAR amplitude. DA describes the temporal variation of physical properties of the ground targets and is used as an indicator for their stability. In the Delta landscape, close-to-zero amplitude and large DA corresponds to water bodies with no electromagnetic energy being reflected back to the radar sensor. Low amplitude and large DA are usually associated with vegetation due to volumetric scattering. High amplitude and small DA are found at man-made structures and bare rocks whose dielectric constants are comparatively large and vary little during time unless being destroyed or damaged.

We extracted DA with substantial amplitude (e.g., >0.025) to exclude pixels in the water. The selected targets may contain vegetated cover, natural bare earth, and manmade structures such as levees and buildings. High DA may be associated with construction, damage, or renovation of roads and other structures or agricultural activities.

Results

Volumetric decorrelation and temporal decorrelation are primarily responsible for low coherence in the Delta. To investigate the relationship between the interferometric coherence and temporal intervals of C-band spaceborne Sentinel-1 data over McDonald Island, we generated 821 interferograms and coherence maps with temporal intervals between 6 and 72 days during 12/31/2014-11/17/2019 from descending path 42. The average coherence decreases rapidly with increasing temporal intervals (Figure A-1). The interferograms with temporal intervals greater than 30 days exhibit a similar level of low coherence (<0.2).

Figure A-1: The Relationship between the Coherence and the Temporal Intervals Spanned by Interferograms Derived from Sentinel-1 Data

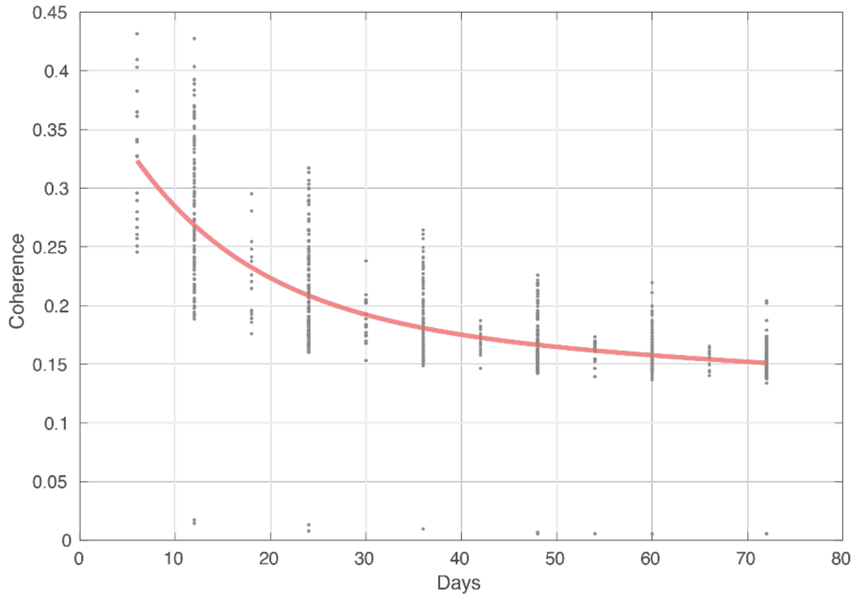

Figure A-2 shows the mean and standard deviation of the amplitude and DA derived from Sentinel-1 path 35 over McDonald Island. Water has the least amplitude, and the largest DA. Agricultural fields clearly delineated by their angular outlines have low amplitude and large DA. Buildings in the island have outstandingly high amplitude and small DA.

Figure A-2: The Mean and Standard Deviation of the Amplitude, and the Amplitude Dispersion (DA) over McDonald Island

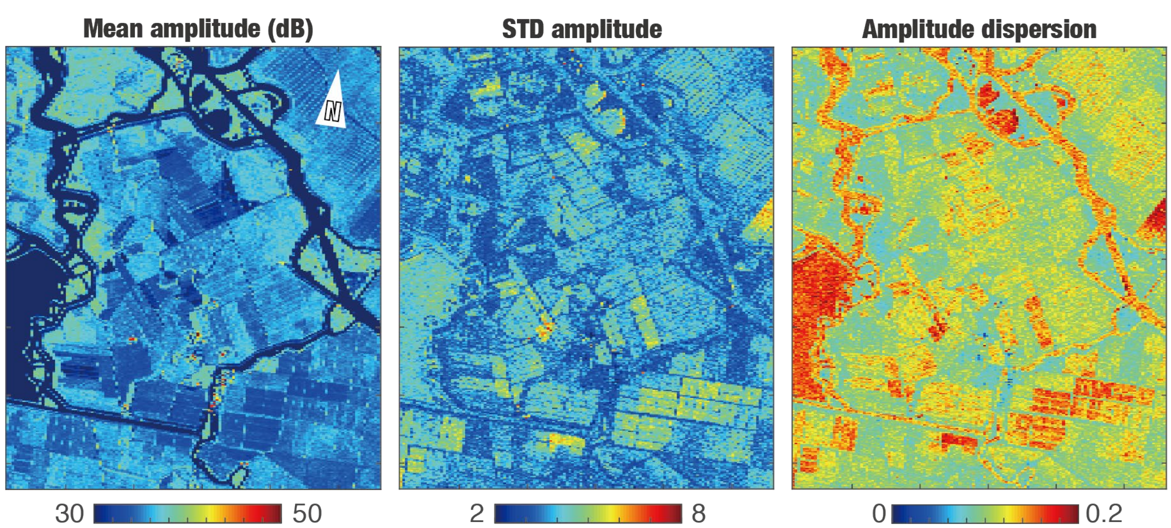

The maps are in radar coordinates of Sentinel-1 path 35.

The levees along McDonald Island are our primary research interests. We extracted the InSAR-derived displacement and DA along the levees. The high gradients in the displacement map (color changes in Figure A-3a) and the high DA (reddish targets in Figure A-3b) show suspicious segments that might be associated with land cover changes and/or levee instability.

Figure A-3: The Relative Vertical Motion and the Amplitude Dispersion (DA) along the McDonald Island Boundaries Derived from Sentinel-1 Data

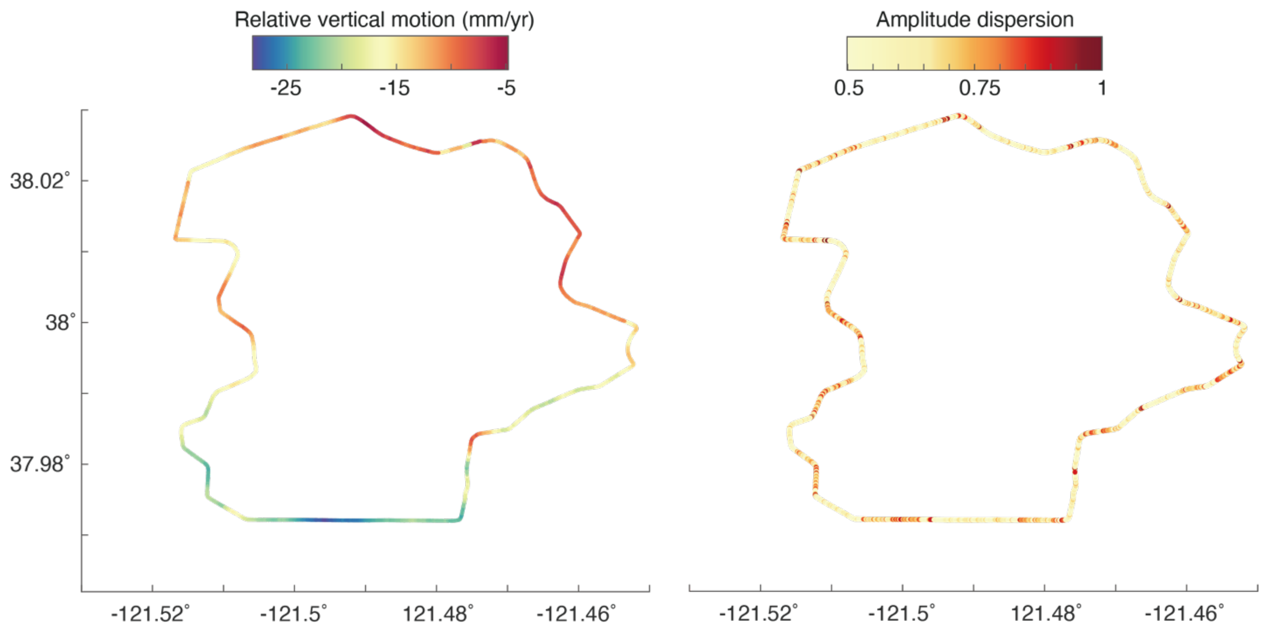

High-resolution UAVSAR results

Similar to the results from Sentinel-1, the bounding levees and man-made structures inside the island show relatively high coherence. Water bodies present low SAR amplitude and large DA. An example interferogram spanning only 19 days during 11/8/2018-11/27/2018 (Figure A-4) does not present evident deformation signals.

Figure A-4: (a) Average Coherence Map from UAVSAR. Man-made Structures Usually Maintain Stable Reflectivity and Exhibit High Coherence (Bright Color); (b) An Example of Interferogram Generated by Two Scenes collected on 11/8/2018 and 11/27/2018

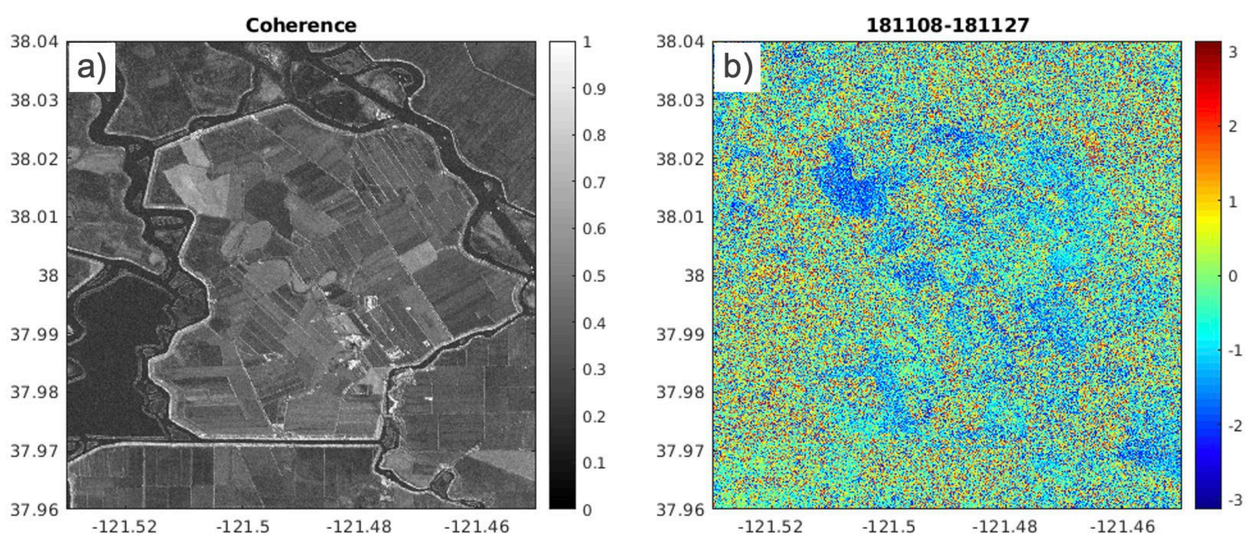

One color fringe (-π to π) represents displacement by 11.9cm (half of wavelength) along the radar line-of-sight.

Flight line #15503 represents one of the largest UAVSAR data collections over the Delta. A total of 64 scenes were collected from 07/18/2009 to 11/14/2017 (Figure A-5a). This allows us to investigate potential seasonality in the amplitude and coherence. For the coherence analysis of data pairs, we applied a temporal threshold of one season, i.e., 90 days, and generated 98 coherence maps. The median coherence decreased nonlinearly from 0.6 to 0.2 from about 20 to 90 days of temporal intervals (Figure A-5b).

Figure A-5: (a) Data Pairs for the Interferograms and Coherence Maps for Flight Line #15503. Each Horizontal Line indicates One Image Pair with the Acquisition Dates referring to the X Axis; (b) The Relationship between the Median Coherence and the Temporal Intervals in Days

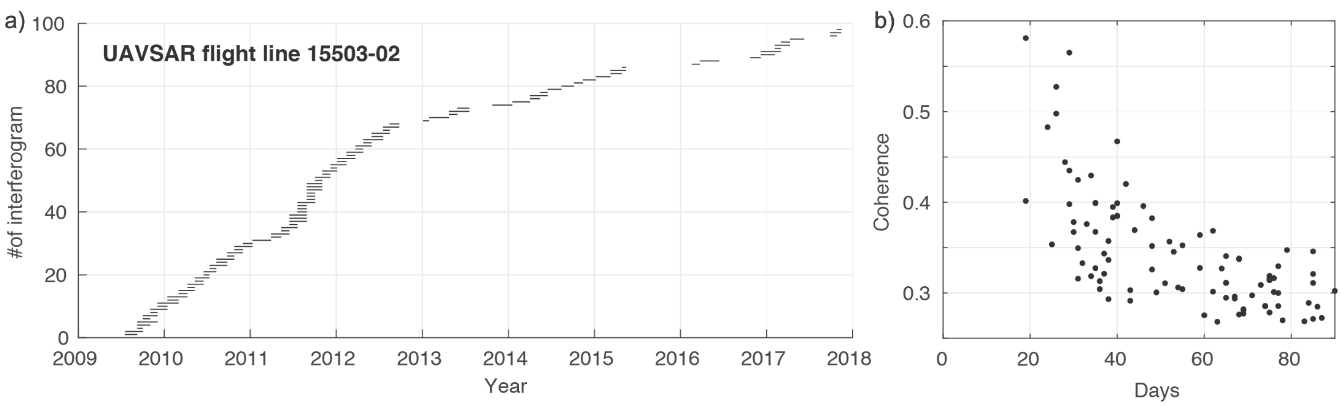

a b

The researchers fitted the corresponding amplitude time series from 64 acquisition dates using a sinusoidal function assuming one-year period. The earlier time frame from 2009 to 2012 has relatively higher temporal resolution which allows for resolving apparent seasonal fluctuations. When evaluating the coherence, the researchers assigned the median coherence to the middle date of each of the 98 data pairs. The practice of assigning the coherence to the middle date for variable-length temporal intervals (~20-90 days) may introduce a bias. The research team again fitted the coherence time series using a sinusoidal function. The results show apparent seasonal variations in coherence, yet the cyclic variation in amplitude is still undetermined (Figure A-6). When relying on the results from the sinusoidal fit, the amplitude and the coherence are out of phase: the amplitude declined from mid-Aug to mid-Feb while the coherence dropped from end-Nov to end-May. An increased precipitation during winter to spring in California is likely to cause decorrelation. Variable soil materials, harvest activities, and vegetation likely add uncertainties to our analysis.

Figure A-6: The Time-series of Amplitude and Coherence for Flight Line #15503

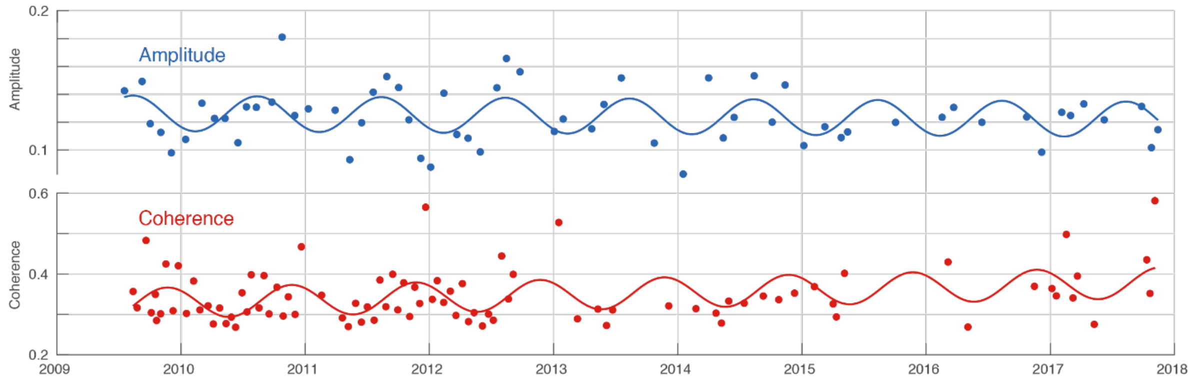

The dots show the measurements with the fitting one-year-period sinusoidal waveforms in the corresponding colors.

Compared with the high SAR amplitude of the buildings in the southern part of the island, SAR amplitude along the levee is moderate (Figure A-7). This may be due to dry clay at the surface as illustrated by the high-resolution Google Earth basemap. The dielectric constant and thus the recorded SAR amplitude of dry clay can be much smaller than that of more saturated and wet clay. Interestingly, the inner roadway bounding the levees represents small amplitude, in a similar amount to that of the surface water, which is likely to be a result of the low-dialectric-constant materials.

Figure A-7: Average Coherence, Amplitude, and the Dispersion of Amplitude (DA) over McDonald Island derived from Three UAVSAR Flight Lines

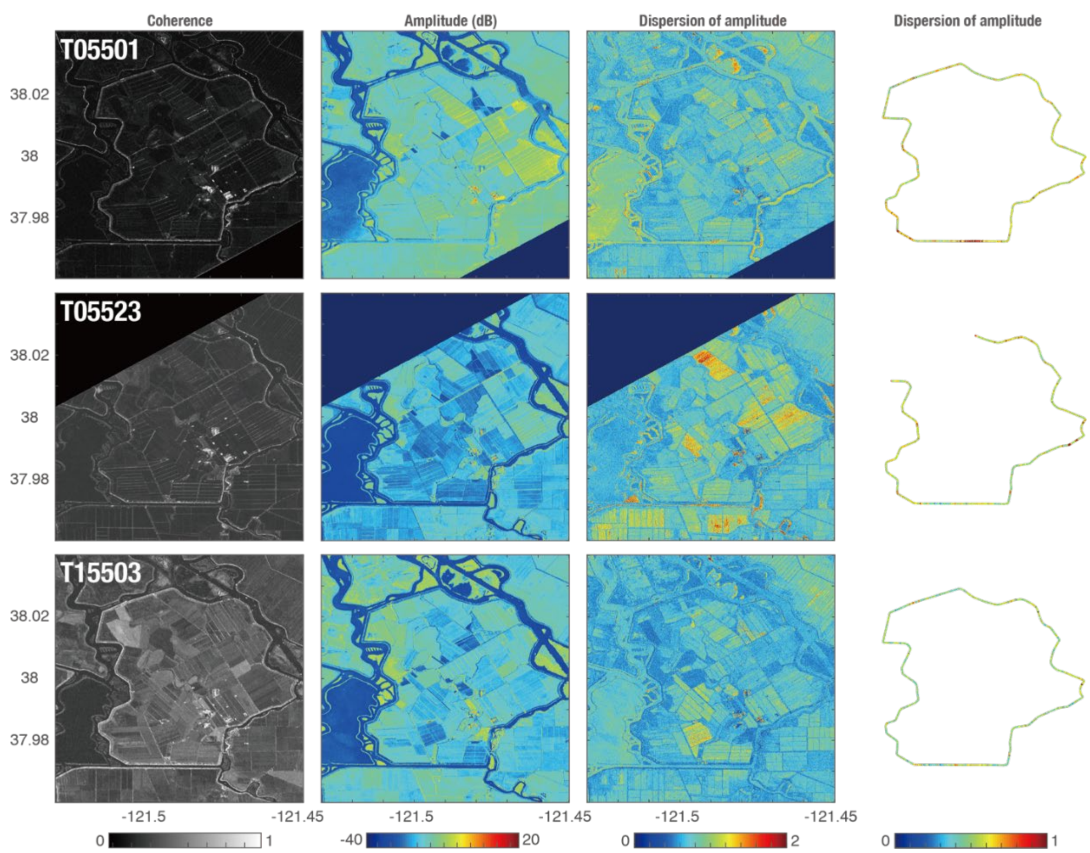

Discussion

Patches with high DA represent agriculture growth and harvest distributed several places in the island. On the other hand, patches with low DA (bluish clusters in Figure A-4) are mainly observed in the southeastern part of the island, and their locations coincide with buildings and infrastructures. The research team didn't find clusters of high-DA targets along the levees, suggesting no collapse or appreciable deformation of the levees during the observing period. Three isolated targets with large DA were selected: T1 is on the levee, and T2 and T3 are contained in the island (Figure A-8). Time-series amplitude show a suspicious amplitude increase around the entrance of a canal at T1 in the end of 2015. In the southern part of the Island, an abrupt increase around 10/21/2016 at T2 is likely due to one-time harvest spanning a couple of months. The subsequent gradual amplitude decrease can be explained by a continuous vegetation growth. Interestingly, time-series amplitudes at T3 show 2-3 fluctuations during 2015-2018 that may be related to seasonal harvests, as illustrated by the high-resolution optical images archived in Google Earth. The limited number of historic images in Google Earth restrict our ability to precisely infer the exact time of harvests.

Figure A-8: (a) The Amplitude Dispersion at High-coherence Targets. (b) The Amplitude Time Series at Three Selected Targets

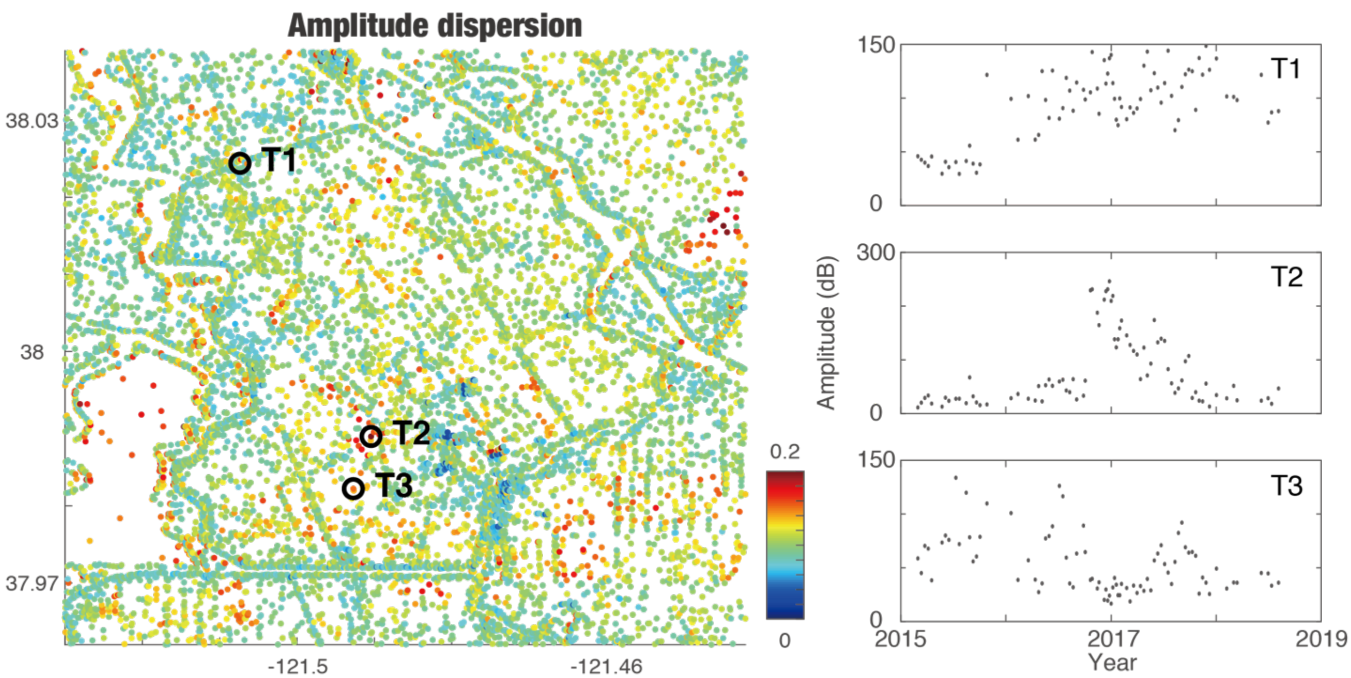

In the results of #05501, the researchers identified a drastic decline in radar amplitude and thus a consequent high DA for two linear features L1 and L2 along the levees in the southwestern part of the island (white boxes in Figure A-9).

Figure A-9: Average Coherence Map, Average Amplitude Map, and Dispersion of Amplitude (DA) Map over McDonald Island. Second Row shows an Enlarged Area in the White Boxes, where Linear Segments (L1 and L2) of High DA on the Top of the Levees are Marked

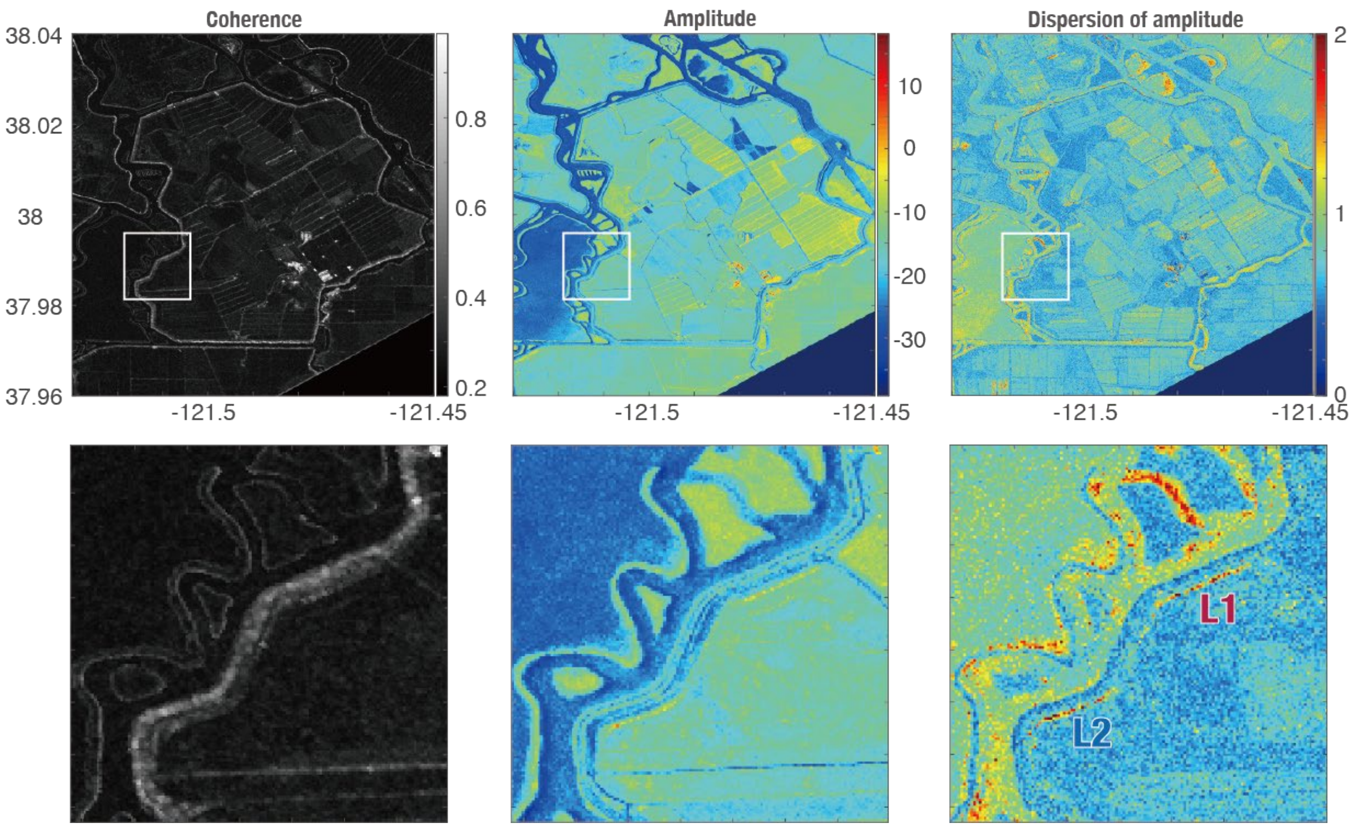

The time-series amplitude at both segments shows abrupt decline by ~15dB in 2009 (Figure A-10). Time-series amplitude after 2009 show moderate variations that may be due to changes in soil moisture and/or growth and removal of vegetated covers.

Figure A-10: Time-series Amplitude of L1 and L2 Segments

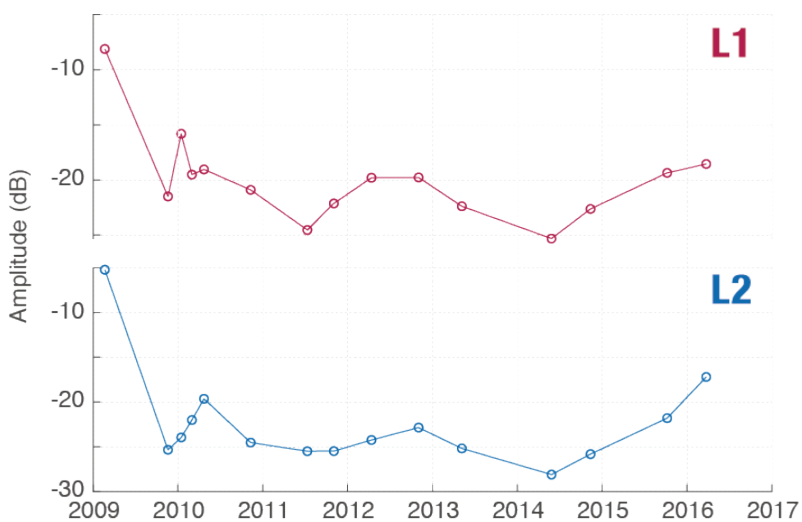

Remarkably, the time of amplitude plunge is consistent with road widening that was implemented in the middle to late 2009, which is determined from the available images in Google Earth. The earliest acquisition time of flight lines #05523 and #15503 is in November 2009 and June 2016, respectively. These two flight lines do not exhibit large DA around this area, confirming that the road widening took place earlier (i.e., before November 2009).

InSAR and its time series analysis are established tools to measure the Earth's surface displacements in various landscapes and associated with different geological processes. Monitoring the regional displacements is promising, especially in urban regions. The southern part of the Delta close to the San Joaquin Valley shows evident subsidence, consistent with previous NASA/UAVSAR results (Bekaert et al., 2019). Widespread land subsidence due to groundwater withdrawal over the San Joaquin Valley has been problematic since the mid-1920s, which may affect the structural integrity of the southern part of the levee system. The McDonald Island is relatively stable without pronounced displacement gradients.

However, InSAR applications in the delta environments is limited by highly varied soil moisture and vegetated covers. Zwieback et al. (2015) reported that a change in soil moisture of 20% contributes to an apparent deformation by more than 2 cm for an L-band airborne SAR system, similar wavelength to that of UAVSAR. Irregular and high-frequency phase changes frequently occur in the Delta not due to ground deformation; instead, they may be a consequence of changes in water content and land cover and/or atmospheric noise. The deformation measurements of the localized islands and levees are associated with large uncertainties due to the coarse resolution of satellite images and the above-mentioned artifacts.

Conclusions

Regional deformation measurement in urban environment can be achieved by InSAR methods at a high accuracy of a few mm/yr when a large collection of SAR images is available. A suggested temporal threshold for C-band spaceborne Sentinel-1 data is less than one month to maintain the coherence in the Delta. A regional displacement pattern over the Delta can be quantified, highlighted by an increasing subsidence to the south where the groundwater depletion occurs in the San Joaquin Valley. However, resolving localized deformation in the delta environment remains to be challenging due to constantly changing soil moistures and vegetated covers from harvest and seasonal growth, as well as atmospheric turbulence.

As a complement, InSAR coherence and SAR amplitude are increasingly used to unveil land cover changes and soil moisture-related processes. The change of amplitude dispersion shows two linear features southwest of McDonald Island that we interpret to be due to road widening. Repeated harvests can be effectively located and traced as well. A joint use of optical and microwave remote sensing images from the ground, air and space and a dense monitoring network of in-situ geophysical and geotechnical tools can help better understand the spatiotemporal development of the levee systems.

ENERGY RESEARCH AND DEVELOPMENT DIVISION

Appendix B: Geophysical Methods for Assessing Levee Integrity

August 2024 | CEC-500-2024-093

APPENDIX B: Geophysical Methods for Assessing Levee Integrity

Introduction

Near surface geophysical surveys were conducted to evaluate the structural integrity of levees at McDonald Island, where levee failure would compromise gas pipelines and other gas infrastructure. Methods included seismic surface wave, electrical resistivity, ground penetrating radar (GPR), and magnetic. Geophysical survey sites were selected after review of soil borehole logs, topographic maps, soil maps, aerial imagery, and InSAR (interferometric synthetic aperture radar) data. The seismic surface wave method was used to obtain estimates of shear wave velocity (Vs). Electrical resistivity surveys were used to distinguish between sandy and clayey soils. GPR provided detailed images of stratigraphy that may help locate parts of the levee affected by rodent burrows. Magnetic surveys were used to verify the location of natural gas supply pipelines and irrigation drains (sumps). The position of geophysical surveys was tied to Department of Water Resources (DWR) distance posts on the levee road with measuring tape. Point locations were also recorded using GPS and used to assign global coordinates.

Seismic surveys were carried out at selected locations on McDonald Island along both the top and bottom of the perimeter levee using the surface wave method. More specifically, we used the two-dimensional multichannel analysis of surface waves (2D MASW) method. Seismic surveys were performed using a land streamer in order to obtain shear wave velocity (Vs) estimates within the levee body and beneath the levee. Of the different geophysical methods used in this study, the seismic method was the most time and labor intensive, however it provides an essential indicator of levee integrity, the Vs.

Electrical resistivity surveys were carried out using a capacitively-coupled dipole (CCD) system to complement seismic surveys. The CCD system is towed while data is recorded, which allows for a very high rate of data acquisition. Magnetic and GPR surveys were carried out using wheeled carts, and also have high rates of data acquisition.

Acquisition parameters for the 2022 surveys are described below:

> Seismic: 2D MASW method, 24 channel landstreamer, 2m geophone spacing, PEG-40 kg impact source, 10m shot spacing. Top and base of levee. Total line length: 4420m.
>
> Resistivity: OhmMapper: 4 receivers, 5m dipole length. Top and base of levee. Total line length: 3000m.
>
> GPR: 100 and 400 MHz. Top of levee. Total line length: 2385m.
>
> Magnetic: Geometrics G-858 cesium vapor magnetometer, dual sensor with cart. Profile length ~ 600m, top and base of levee. Total line length: 3400m.

Images of geophysical profiles are provided, including seismic Vs, electrical resistivity, magnetic intensity, and GPR radargrams. Basemaps showing geophysical line locations are provided. Seismic surface wave data was processed using SeisImager software. Results from seismic surveys are presented as two-dimensional shear wave velocity (Vs) profiles. Resistivity data was processed using OhmImager. Magnetic data was processed using Magmap2000[7]. GPR data were processed using EKKO Project.[8]

Seismic Surveys - 2022

Seismic data were acquired at three sites using the 2D Multichannel Analysis of Surface Waves (MASW) method. Total line length of the sites was 4420m. This was nearly evenly split between sites at the top of the levee (2270m) and sites at the bottom (2150m). Sites at the top of the levee were more exposed to wind than sites at the bottom, and in some cases data quality was affected by wind noise.

Western Site

A new survey site was added in the 2022 surveys at the site of a 1982 levee breach, which occurred on the northwest side of the island. The location of the breach was indicated by the landowner. The top of the levee was surveyed with a single line 1060 meters long, 574A. The base of the levee was surveyed with three shorter lines; 527B, 525B, and 525A (Figure B-1). Data quality at this location was variable due to wind noise, but nearly all data were usable.

Figure B-1: Basemap of Western Site Showing Lines at Top of Levee (527A) and at Bottom (527B, 525B, and 525A). Location of 1982 Breach is Labeled

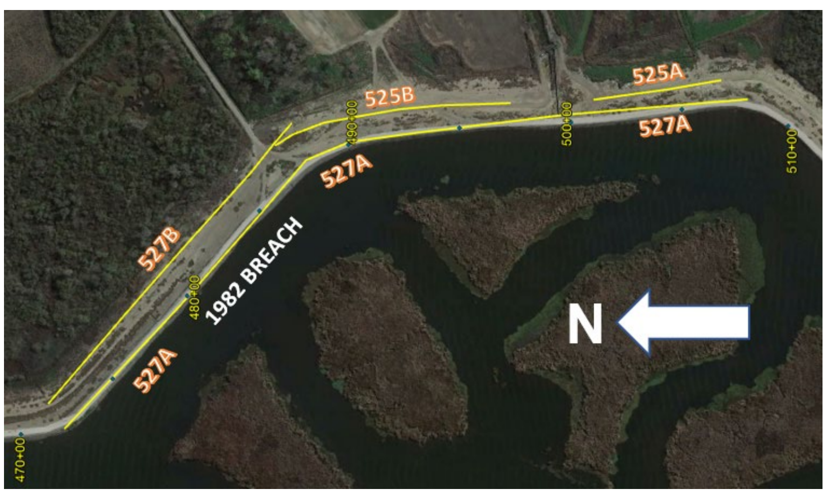

S N

[7] A program that provides basic data processing filters for quick analysis of magnetic, OhmMapper, and EM61 data. MagMapTM facilitates data download from Geometrics magnetometers, applies diurnal correction upon export, and generates 2D/3D color contour plots and shaded relief maps. The program also offers full GPS support with UTM conversion, sensor-GPS antenna offset computation as well as GPS file integration with basic magnetic data. https://www.geometrics.com/software/magmap/

[8] EKKO_Project is the all-inclusive software solution for managing, displaying, processing and interpreting GPR data. https://www.sensoft.ca/products/ekko-project/overview/

Line 527A (partial), top of levee. A portion of the line centered at the 1982 breach is shown. The breach appears to be ~100m wide. The full depth of the breach appears to be 8-10m below the levee surface. The area of the breach shows anomalously high velocities (Figure B-2). Velocities exceed 200 mm/yr (green color) and evidently reflect the presence of repair materials (rock) instead of the low-velocity peat (orange color) on either side of the breach.

Figure B-2: Line 527A (Partial), Top of Levee

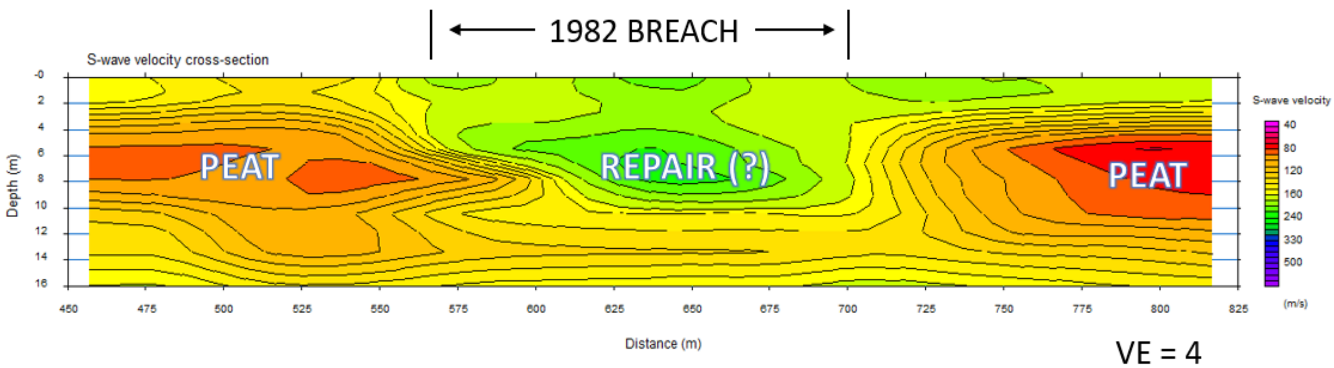

Figure B-3 shows line 527B (partial), base of levee. A portion of the line centered at the 1982 breach is shown. The depth of the breach is only about 2m at this location because the recording surface is at the base of the levee.

Figure B-3: Line 527B (Partial), Base of Levee

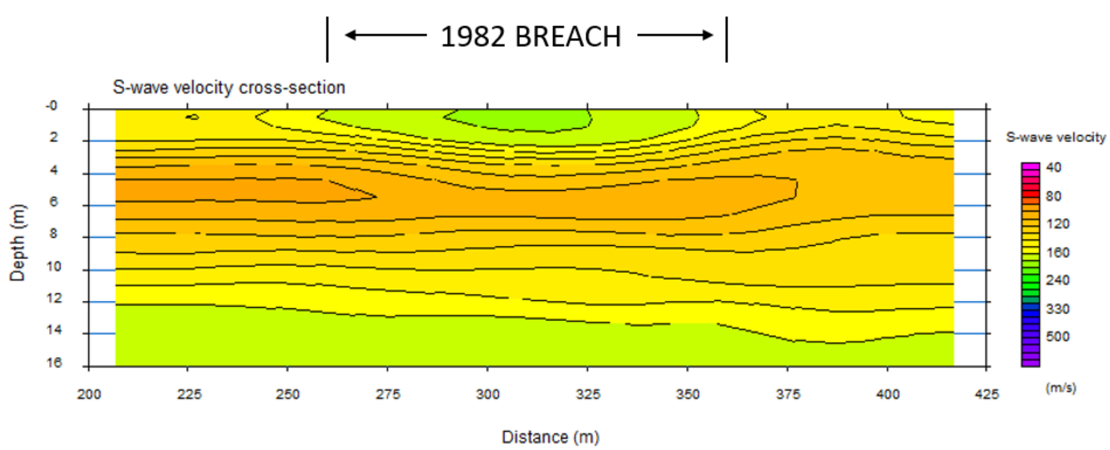

Southern Site

At the southern site, a section of the levee 840m long was surveyed with lines 519 and 524A, both recorded on top of the levee (Figures B-4, B-5, and B-6). A single line 950 meters long was recorded at the base of the levee. The data quality of lines 523A and 524A was good. Data quality of 519 was variable due to wind and an irrigation pump.

Figure B-4: Basemap of Southern Site. Lines 519 (430m) and 524A (410m) are on Top of levee. Line 523A (950m) is at the Base

Figure B-5: Line 524A, Recorded on Top of Levee

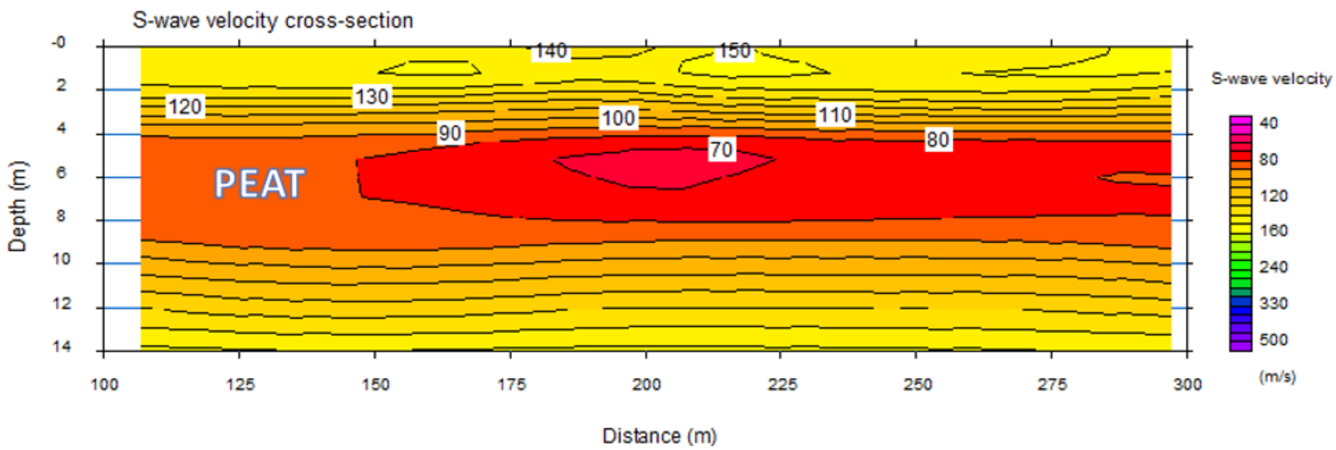

Line 524A, Figure B-5, recorded on top of levee shows Inverted Vs section. Note low-velocity zone at 4-9m depth, this corresponds to a layer of peat up to 5 meters thick underlying the levee. Dark orange color corresponds to very low V_S < 80m/s. Vertical exaggeration (VE) = 4.

Figure B-6: Line 523A (Partial). South Site, Base of Levee

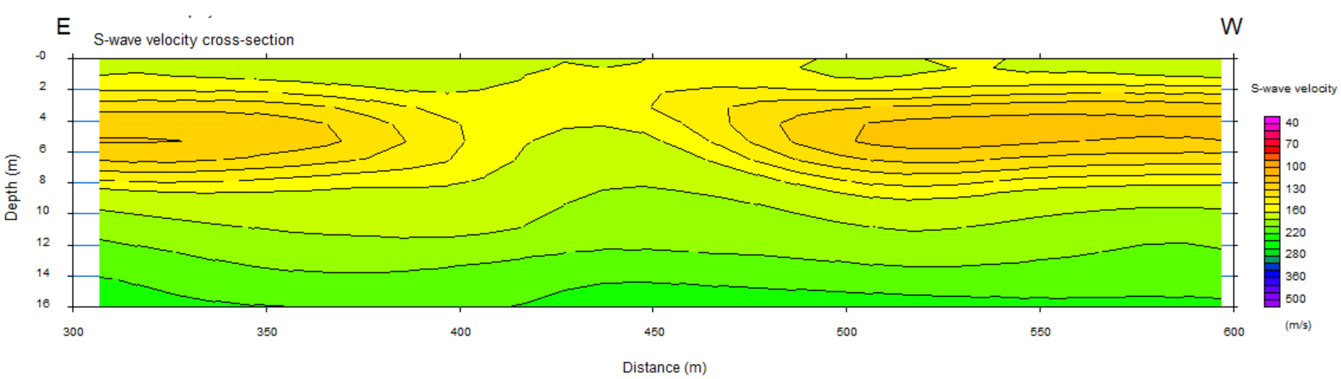

This section shows a lateral break in the low-velocity layer (yellow color) at distance 400-450 m. VE = 4.

Northern Site

Two lines were recorded, 524B on top of the levee (320m) and 523B (430m) at the base (Figure B-7). The top of the levee at this site was often exposed to strong wind and data quality was occasionally affected. Line 524B (top) is centered over an old tidal channel and coincides with a 2019 line. Line 523B (bottom) extends coverage to the west of a 2019 line.

Figure B-7: Basemap of Northern Site, Showing Lines 523B (Base of Levee) and 524B (Top)

Figure B-8 shows line 524B, top of levee. SW to left and NE to right. The central section, from a distance of 100m to 200m (yellow colors), shows a high-velocity zone at depths greater than 8m, with Vs > 130m/s. This line (and the levee) crosses the axis of Whiskey Slough. The higher velocities may be due to coarser-grained channel sediments. The upper 2m of section (green color) has higher velocities than the underlying material and corresponds to levee fill material.

Figure B-8: Line 524B, Top of Levee

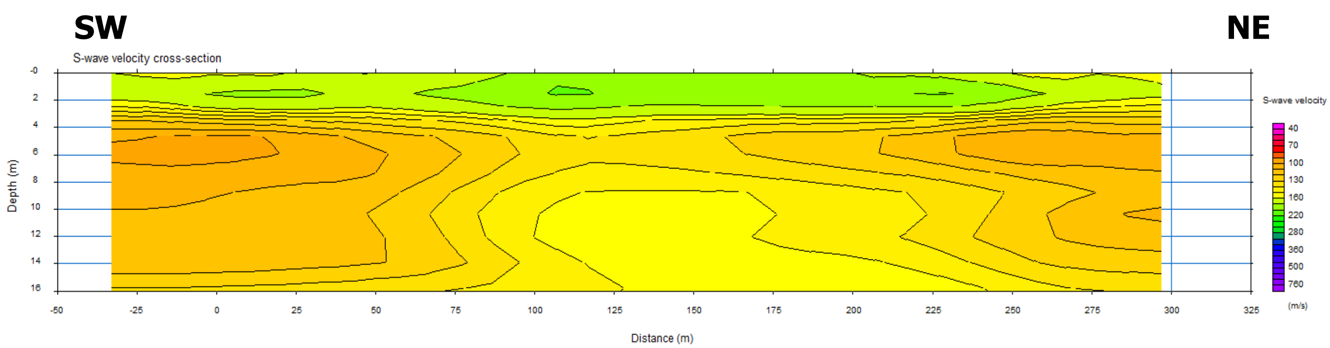

Figure B-9 shows the base of the levee for line 523B. Note the low-velocity zone at the left end of the line, depths of 4-6m, dark-orange to red color. This has Vs < 100m/s and corresponds to peat.

Figure B-9: Line 523B. Base of Levee

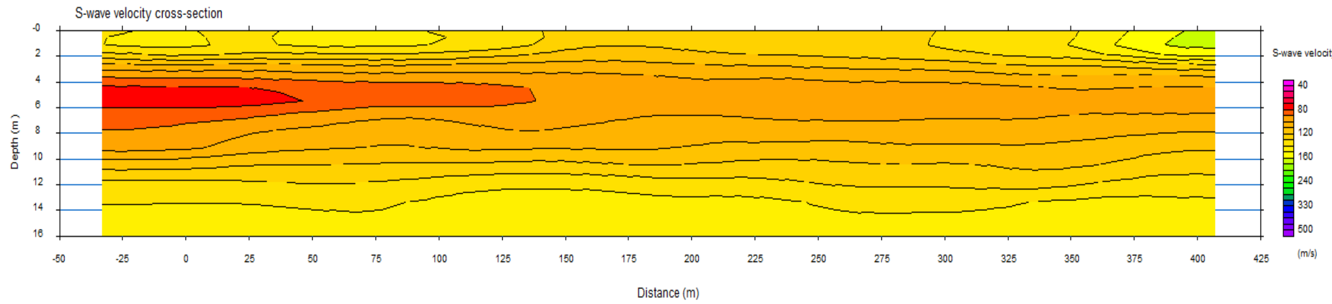

Electrical Resistivity Surveys

Electrical resistivity surveys were recorded along both crown and toe of the levee at each of three sites during both the 2019 and 2022 surveys. The examples below are from the 2019 surveys.

The first site is located north edge of McDonald Island, where a tidal channel intersects the edge of the island The second site is located along the southern edge of the island in a location that was identified as having a high subsidence rate based on InSAR data. The third site is on the eastern side of the island in an area that is believed to be stable based on InSAR.

Resistivity surveys were performed at each of the sites using an OhmMapper 4-receiver CCD system. A total of six profiles was recorded, ranging in length from 400 to 1000m (Figure B-10).

Figure B-10: Electrical Resistivity Profile along Top of Levee, Northern Site

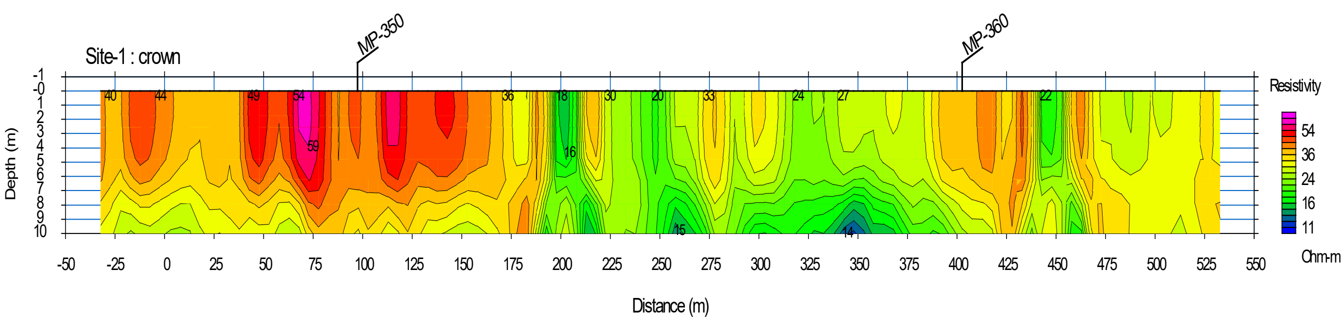

Ground Penetrating Radar

GPR surveys were carried out in 2019 at the same sites where seismic and electrical resistivity surveys were performed, as described above. GPR profiles were 300m long, recorded along the crown (top) of the levee at all sites and along the toe (bottom) of the levee at two sites. GPR data were recorded using 100MHz antennas and a step size of 1m. Sample profiles are shown below in Figures B-11 and B-12.

Northern Site

Figure B-11: Basemap Showing GPR Line Locations at Northern Site (Site 1)

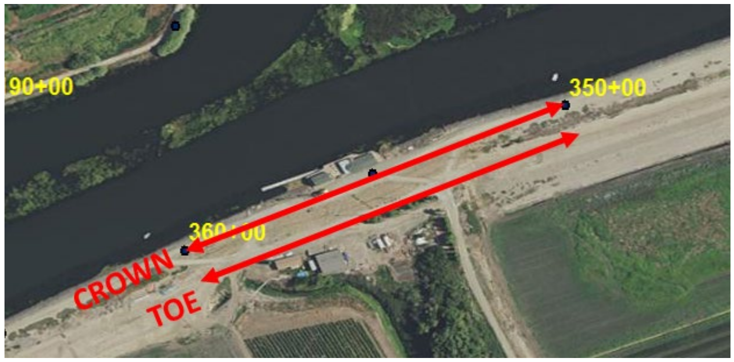

GPR lines in red along crown and toe of levee. Yellow numerals are 1000-foot DWR stations.

West Site

Figure B-12: Survey Basemap at Site 3, McDonald Island

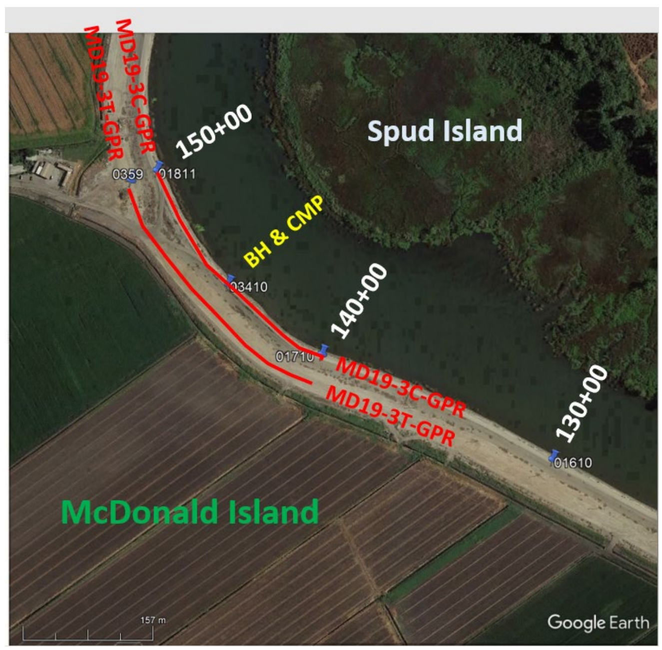

GPR profiles in red along crown and toe of levee. White numerals are 1000-foot DWR stations.

Figure B-13 shows A short, thick, dipping reflector is present on the left-hand side of the profile. Thinner channel-like features are in the central portion of the profile. Profile length is 300m.

Figure B-13: Ground Penetrating Radar Profile,
Site 3 (Eastern Side of Island), Along Levee Toe

SE **NW**

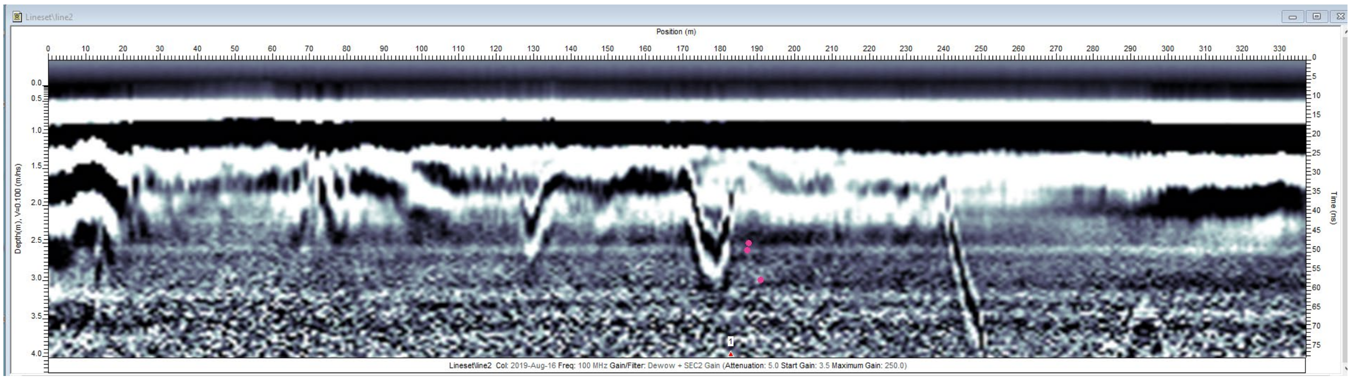

CALIFORNIA ENERGY COMMISSION

ENERGY RESEARCH AND DEVELOPMENT DIVISION

Appendix C: Levee Risk Assessment

August 2024 | CEC-500-2024-093

APPENDIX C:
Levee Risk Assessment

The risk assessment for McDonald Island was completed using the level crossing statistical method. This appendix addresses the work to develop the updated seismic fragility functions of Bacon Island which is adjacent to McDonald Island. There are two reasons to update fragility functions for Bacon Island: 1) Introduce more accurate and realistic material divisions within levee cress-section and assign various undrained shear strength to fine-grained soil in different zones; 2) Refine the site characterization analysis of Bacon Island levees based on the standard penetration test (SPT), cone penetration test (CPT), laboratory test, and geophysical test within the entire island.

Figure C-1 shows the material division of the northern levee of Bacon Island in the previous model, and there are totally 9 materials being considered within the levee. Apparently, in the Figure C-1, for fine-grained soil materials (e.g., clay and peat), uniform undrained shear strength was assigned to each soil layer. However, undrained shear strength depends on in-situ effective stress and effective stresses vary in different zones within the levee cross-section. At the same elevation level, the effective stress of the site right underneath levee crest is much larger than the effective stress of the site in free field area. Therefore, it is necessary to introduce more material divisions to better capture soil dynamic property of levee and make the model more accurate and reasonable in predicting levee crest displacements during earthquake.

Figure C-1: Northern Levee Cross-section Mesh and Soil Material Divisions in the Previous Model

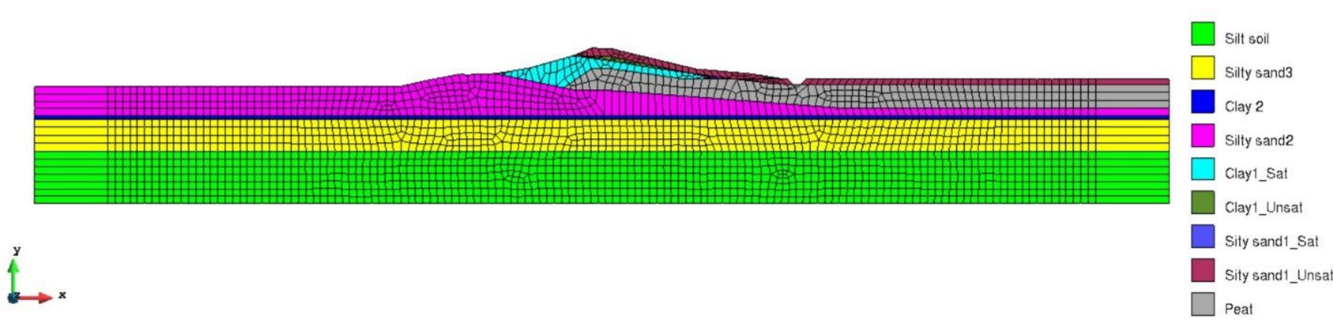

Figure C-2 shows the northern levee cross-section finite element mesh in the new model with 17 materials, and the levee is manually divided into five zones where undrained shear strength of fine-grained materials is calculated separately as a function of consolidation stress. The southern levee will also be analyzed and has potentially higher seismic risk due to its large portion of organic peat soil within the levee cross-section.

Figure C-2: Northern Levee Cross-section Mesh and Soil Material Divisions in the New Model

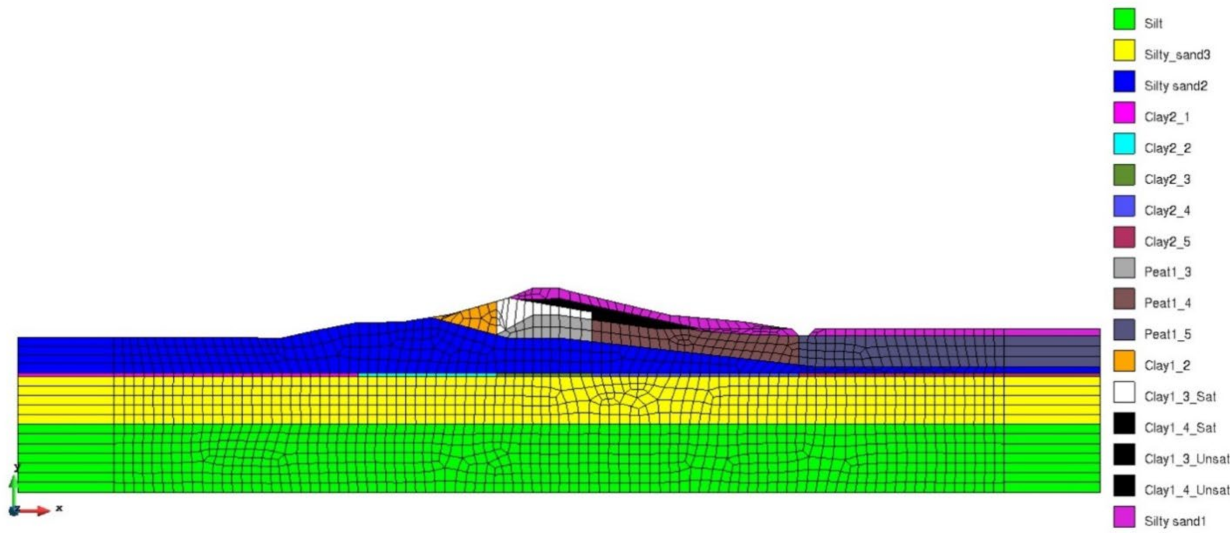

Figure C-3 presents the southern levee cross-section mesh with 20 materials in 5 zones within the levee.

Figure C-3: Southern Levee Cross-section Mesh and Material Divisions within Levee

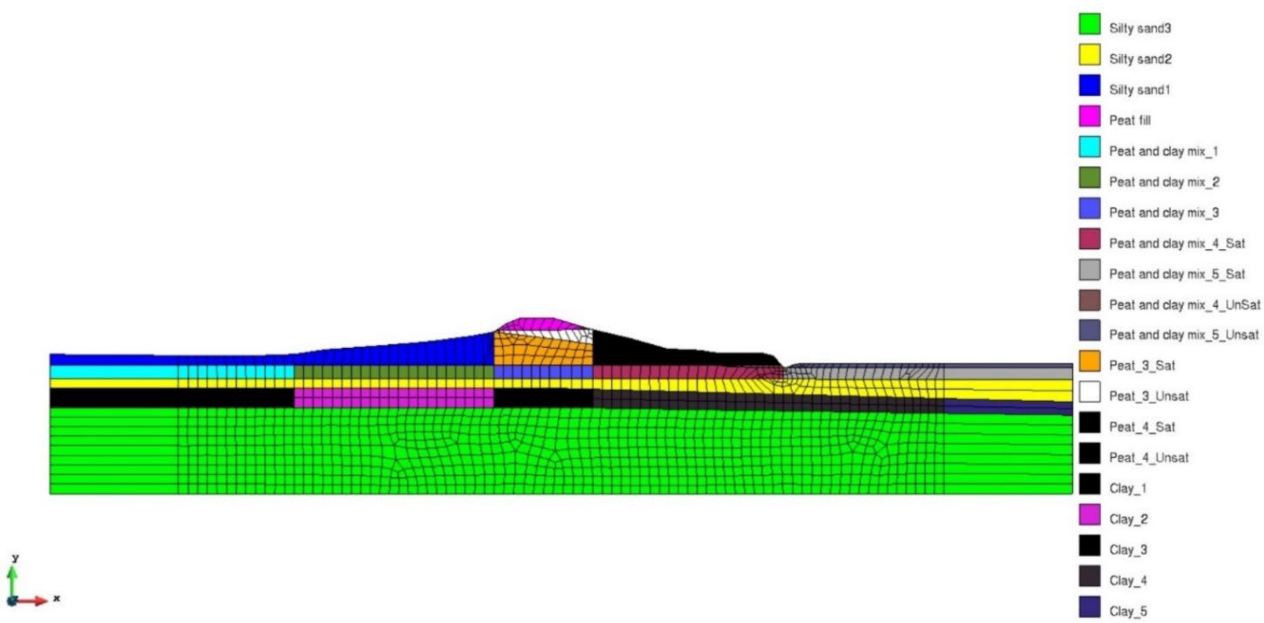

Site characterization is relatively important in levee fragility function development where we assess levee crest vertical displacement versus crest peak ground velocity. In the previous northern model, we interpreted soil shear strength using data from cone penetration tests (CPT's) implemented on the levee crest. The cone factor N_{kt}, which relates CPT tip resistance to undrained strength, was assumed to be 14 for all soil and then calculate shear strength, which is not sufficiently reasonable since N_{kt} varies in different soil. To avoid making this rough assumption, we decide to calibrate N_{kt} of different soils based on CPT tip resistance and laboratory strength tests. We utilize four triaxial unconsolidated undrained tests of soil samples from northern and southern levees to obtain lab-measured shear strength and iterate N_{kt} values for these soils until CPT- interpreted shear strength matches lab-measured undrained shear strength. Additionally, we then calculate the in-situ shear strength ratio (shear strength divided by effective stress) for these fine-grained soils, and shear strength ratio can be utilized to compute in-situ shear strength of soil in different zones. Table C-1 summarizes calculated cone factor N_{kt} and shear strength ratio based on CPT and triaxial unconsolidated undrained (TUU) test results.

Table C-1: Shear Strength Ratio and Cone Factor Profile Based on CPT and TUU Test Results

Location	Soil type	Depth (ft)	Shear Strength S_u(psf)	Total stress σ_v (psf)	Effective stress σ_v' (psf)	Tip resistance q_t (psf)	Shear Strength ratio S_u/σ_v'	Cone factor N_{kt}
North	Peat	30	1206	2519.6	1058.6	8502.1	1.14	5.0
South	Peat	10	498	786	399	2157.0	1.25	2.8
South	Clay	20	669	1536	526.8	9313.8	1.27	11.6
South	Clay	25	473	2020.9	697.3	4684.8	0.68	5.6

Table C-1 demonstrates that cone factor N_{kt} is smaller for peat than cone factor in clay. Based on the shear strength ratio in the Table C-1, we update the undrained shear strength of fine-grained soil in the northern levee. Table C-2 shows the results of calculated undrained shear strength of soil within northern levee. According to Table C-2, the highest undrained shear strength of same soil appears in Zone 3, and undrained shear strength of lower clay is higher than upper clay.

Table C-2: Updated Undrained Shear Strength of Fine-grained Soil in the Northern Levee

Zone	Soil	Undrained shear strength (kPa)
1	Lower clay	47.1
2	Upper clay Lower clay	8.6 67.3
3	Upper clay Peat Lower Clay	35.7 33.5 86.6
4	Upper clay Peat Lower Clay	29.4 25.2 56

Zone	Soil	Undrained shear strength (kPa)
5	Peat Lower Clay	17.6 30.5

In addition, there are two triaxial consolidation undrained (TCU) tests of soil samples from northern levee and we can acquire normally consolidated shear strength ratio of soil. Tables C-3 and C-4 show the two triaxial consolidation undrained test results. Normally consolidated shear strength ratio $(S_u/\sigma_v')_{nc}$ of peat and clay in northern levee are relatively close.

Table C-3: TCU Test of Clay in Northern Levee

Soil	Sample	In-situ effective stress (psf)	Consolidation pressure (psf)	σ_1' (psf)	σ_3' (psf)	(S_u/σ_v')	$(S_u/\sigma_v')_{nc}$
Clay	A	893.1	910	1414	104	0.72	0.48
	B	893.1	1351	2056	559	0.55	
	C	893.1	2350	3000	737	0.48	

psf = pounds per square foot

Table C-4: TCU Test of Peat in Northern Levee

Soil	Sample	In-situ effective stress (psf)	Consolidation pressure (psf)	σ_1' (psf)	σ_3' (psf)	(S_u/σ_v')	$(S_u/\sigma_v')_{nc}$
Peat	A	1058.6	1090	1707	312	0.64	0.46
	B	1058.6	1701	2051	491	0.46	
	C	1058.6	2500	3025	743	0.46	

psf = pounds per square foot

In earthquake dynamic analysis, another important soil property is the modulus reduction relationship (modulus reduction versus shear strain) under cyclic loading and its corresponding backbone curve (shear versus strain). In the previous model, we did not specify modulus reduction model for soil in OpenSees. In the new model, we utilized the modulus reduction and damping (MRD) curves, MRD Unified Model by Darendeli (2001), MRD Unified Model by Menq (2003), and MRD model by Wang et al. (2022) combined with hybrid correction procedure proposed by Yee et al. (2013) for clay, sand, and peat, respectively. The reason that we would like to implement hybrid correction procedure besides three MRD models is that soil backbone curves developed from these three models do not work well in large shear strain portion (generally, if shear strain $\gamma > 0.3\%$), so Yee et al. correction procedure aims to modify the modulus reduction curve in the large strain portion and makes derived soil backbone curve asymptotically approach to assigned undrained shear strength as shear strain increase. Small-strain shear modulus G_{max} is a crucial parameter in quantifying soil shear-strain relationship under cyclic loading, and it can be calculated by using the following equation:

$$G_{max} = \rho^2 * Vs$$

Where ρ is the soil density and Vs shear wave velocity.

Figure C-4 shows results of 3-D presentation of data acquired from Bacon Island northern levee, including shear wave velocity (Vs) and electrical resistivity. We interpret the soil Vs from these geophysical tests and soil density can be calculated from laboratory test.

Figure C-4: Results of 3-D Presentation of Data Acquired from Bacon Island Northern Levee, Including Vs and Electrical Resistivities.

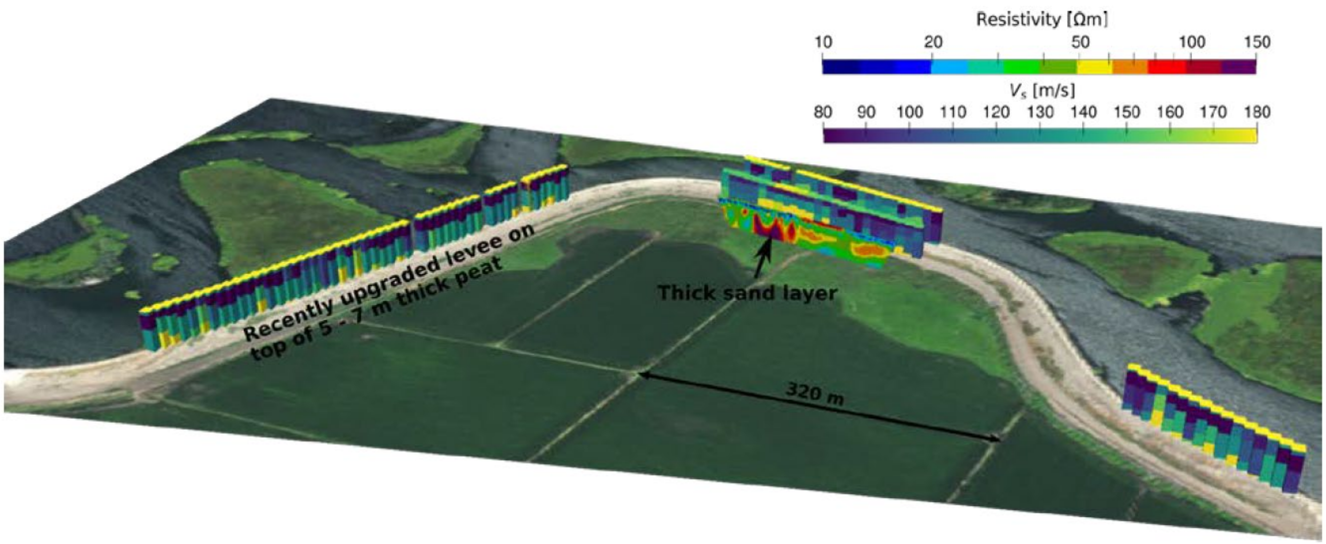

Table C-5 summarizes the results of interpreted soil density, Vs, and G_{max}.

Table C-5: Interpreted Soil Density, Shear Wave Velocity and Small-strain Shear Modulus in Northern Levee

Soil	Density, ρ (kg/m^3)	Shear wave velocity, V_s (m/s)	G_{max} (kPa)
Silty sand, loose	1928.6	160	49371
Gray fat clay, soft	1340.0	120	19296
Black peat, soft	1078.0	80	6899
Silty sand, dense	1980.7	160	50707
Lean clay, stiff	1980.7	150	44566
Silty sand, very dense	1980.7	165	53925
Silt, very stiff	1830.6	180	59312

kg/m^3 = kilogram per meter cubed; m/s = meter per second; kPa = kilopascal

After acquiring G_{max} for soils within the levee, we then implement these MRD models and correction procedure to determine modulus reduction curve for these soils. Figure 16 shows the results of derived backbone curves of silty sand, clay, and peat for nonlinear ground response analysis. The undrained shear strengths of silty sand, clay and peat are 12.0kPa, 29.4kPa, and 33.5 kPa, respectively. According to Figure C-5, Yee et al. correction procedure drags backbone curves converge to undrained shear strengths in large shear strain section, which is more reasonable in soil nonlinear ground response analysis.

Figure C-5: (a) Backbone Curves of Upper Silty Sand in the Northern Levee using Menq Model and Yee Correction Procedure; (b) Backbone Curves of Upper Clay in the Northern Levee using Darendeli Model and Yee Correction Procedure; (c) Backbone Curves of Peat in the Northern Levee using Wang Model and Yee Correction Procedure

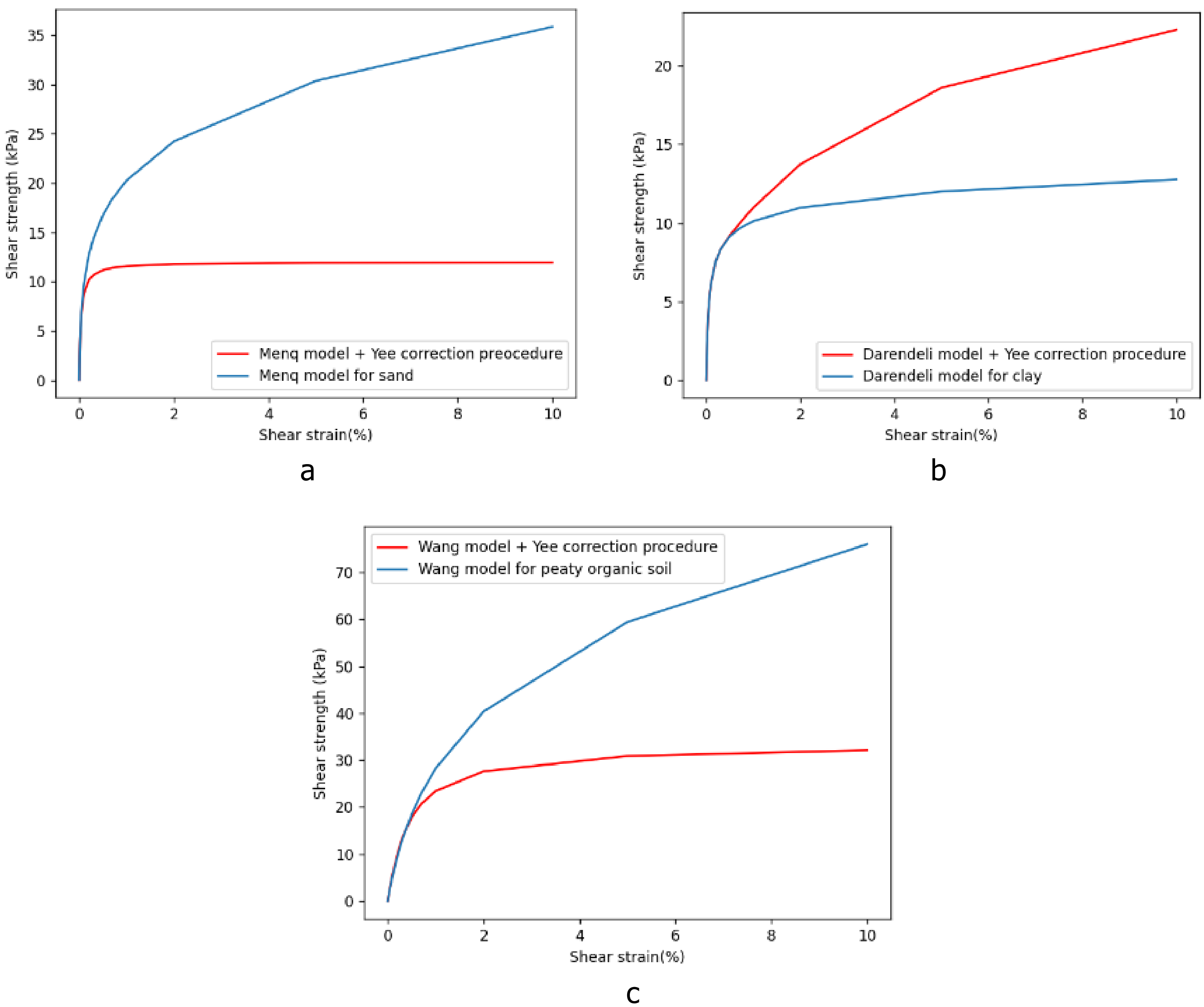

After completing these updates and modifications on finite element models of Bacon Island levee, the researchers believe new models can yield more accurate and reliable results of levee seismic fragility functions. The next step to do is running the updated model of northern levee in OpenSees, comparing results with ones derived from the previous model, and finishing fragility functions of southern levee as well.